Master's thesis

NTNU
Norwegian University of Science and Technology
Faculty of Engineering
Department of Civil and Environmental Engineering

Kyle Lambert

Usability of Extrapolation Methods of Wind Speed Profiles in the Arctic

Can automatic weather station data be used for determining wind energy feasibility?

Master's thesis in Cold Climate Engineering
Supervisor: Knut Høyland, Anna Sjöblom, Matthias Henkies
Co-supervisor: Jukka Tuhkuri
June 2023

NTNU
Norwegian University of Science and Technology

UNIS
The University Centre in Svalbard

Kyle Lambert

Usability of Extrapolation Methods of Wind Speed Profiles in the Arctic

Can automatic weather station data be used for determining wind energy feasibility?

Master's thesis in Cold Climate Engineering
Supervisor: Knut Høyland, Anna Sjöblom, Matthias Henkies
Co-supervisor: Jukka Tuhkuri
June 2023

Norwegian University of Science and Technology
Faculty of Engineering
Department of Civil and Environmental Engineering

NTNU
Norwegian University of
Science and Technology

Acknowledgements

There are many I wish to thank, for their support, ideas, or simply tagging along for the ride while writing this thesis. First, I must give a shout-out to the tremendous Masters of Disasters who made the office vibes jolly, memorable, and generally invigorating. Without them, I would have skied more and wrote less. This leads me to mention Matthias Henkies who called out my love of skiing from the start. Much thanks to him for the open door, always willing to discuss as I wrestled with python scripts and new concepts. Thank you to Anna Sjöblom for the guidance and inspiration throughout my studies and writing. Thank you to Knut Høyland also for his calm mentorship throughout my masters studies. A special thanks to the UNIS Arctic Technology department for welcoming me in, especially the PhD students Arthur, Jules, Malin, and Stig. Thursday coffee and cake meetings are a wonderful tradition which I hope continues. Also a thank you to Jukka Tuhkuri for advice in my studies at Aalto and support in the Cold Climate Engineering program.

For my time at UNIS I have many to thank. A special thanks the ski gang, Anya, Hugo, and Linus, for countless ski adventures. Each one refreshed me to push on writing and made my time here the incredible experience it was. Oliver, a special thanks to you for Friday Gathering, the late night conversations and scooter work sessions. Renee, Anne, and Bryan, thank you for encouragement throughout writing and the cozy autumn semester. Thank you to the Student Council team for embracing my optimism and making a fun semester. Then there is the support from back home. Mark, thank you and don't forget the photo I hung at my desk. I would not have made it here without my family, especially my parents who made the difference. Thank you for always encouraging me to pursue adventure, dream with curiosity, and not give up. A tremendous thanks Annie for supporting this adventure long before it started and sticking by the whole way through. Thank you for putting up with the time difference and call drops and sending endless letters. Much love to you as you carry on the masters student path. And thanks to the many other friends and students who made living in Elvesletta so wonderful. Svalbard and the rest of the Arctic will always call and I very much look forward to coming back to the magical beauty of the far north.

Abstract

Renewable energy is ever increasing in the modern energy grid with a growing portion from wind. Arctic communities are still largely dependent on fossil fuels, with up to 79% entirely dependent on diesel. Therein lies irony as arctic regions experience the effects of climate change up to 7 times greater than worldwide. Wind turbine design requires knowledge of horizontal wind speed at the hub height to estimate annual energy production. Such wind profiles can be studied using LiDAR data. However, LiDAR experiments are expensive to conduct. To cut costs and rapidly evaluate potential wind energy generation sites, extrapolation methods are applied to pre-existing wind speed measurements taken at a standard 10 m height. Wind speed profiles are constructed from measurements taken in Adventdalen on Svalbard during the summer of 2022 using an automatic weather station (AWS) and LiDAR. The LiDAR constructed profiles are a baseline for comparison while the AWS data is used solely to construct model profiles. Four models are evaluated: the power law following IEC-64100-3 standard, a power law variation proposed by Sedefian, the log law, and log law with stability correction. The models are found to be dependent on stability as previously found in other regions. However, the LiDAR baseline shows a decrease in wind speed with height making all models tested difficult to use. It is also found that the IEC method largely overestimates wind speed. The power law proposed by Sedefian is found to perform similarly to the log law with stability correction. The log law with stability correction is more sensitive to input parameters and therefore less robust against less sophisticated instrumentation. The Sedefian variation is found to be the least sensitive to wind speed errors.

Table of Contents

List of Figures **iii**

List of Tables **iv**

Abbreviations and List of Variables **1**

1 Introduction **2**

2 Background **4**

2.1 Arctic Energy Resources and Development 4

2.2 Use of Automatic Weather Station Data 5

2.3 Boundary Layer Wind Speed Profiles 6

2.3.1 Power Law 6

2.3.2 Log Law 8

2.3.3 Stability Considerations 8

2.4 Use of LiDAR Data 9

2.5 Summary and Project Goal 9

3 Method **11**

3.1 Location 11

3.2 LiDAR 11

3.2.1 Data-collection 12

3.2.2 Processing 12

3.2.3 LiDAR Wind Speed Profile Construction 14

3.3 Automatic Weather Station 15

3.4 Pre-processing 15

3.5 Model Profiles Construction 17

3.5.1 Stability Considerations 18

3.6 Wind Energy Potential 19

3.7 Study Cases 19

4 Results **21**

4.1 Wind Conditions 21

4.1.1 Data Availability 21

4.1.2 Direction 21

4.1.3 Stability Classes 23

4.2 All Wind Profiles 24
4.3 Effect of Up Valley vs Down Valley Flow 28
4.4 Effect of Stability 29
4.5 Effect of Wind Speed 32

5 Discussion **36**

5.0.1 Baseline LiDAR Profiles 36
5.1 Study Case Findings 36
5.1.1 Up vs Down Valley Flow 36
5.1.2 Stability 37
5.1.3 Wind Speed 38
5.2 Models 39
5.2.1 IEC Power Law 39
5.2.2 Sedefian Model 40
5.2.3 Log Law 40

6 Conclusion **41**

Bibliography **42**

List of Figures

1 Roughness length calculated near neutral values using AWS data at 2 m and 10 m heights. 7

2 Location of the LiDAR (purple) and AWS (black). The red arrows indicate the down and up valley scan headings and reach. (Norwegian Polar Institute, n.d.) . . 11

3 LiDAR processing steps. Solid gray blocks are inputs/outputs. Solid gold blocks are data handling steps. Gold bordered blocks are filters. 12

4 CNR and radial speed on 2022-07-15 19:18:02 - 19:19:31 UTC 13

5 Selection slices of an example RHI scan for calculating median vertical profile of horizontal wind speed. Taken on 2022-07-15 19:18:02 - 19:19:31 UTC 14

6 LiDAR and AWS data pre-processing steps. Colored paths indicated the use of specific datasets. Solid gray blocks are inputs/outputs. Solid gold blocks are data handling steps. Gold bordered blocks are filters. 16

7 Wind direction correlation at 10 m to 10 m, 100 m, and 150 m heights 22

8 Time series of wind direction at 10 m, 100 m, 150 m heights 22

9 Stability classes based off 2m and 10m heights 23

10 Model to LiDAR profile correlation for all suitable profiles at 80 m height 24

11 Median wind speed for all suitable profiles 25

12 Median difference of models to LiDAR wind speed for all suitable profiles 25

13 Percent distribution of difference in model vs LiDAR wind speed for all suitable profiles at 80m height 26

14 Median wind power density for all case 27

15 Comparison of power density profiles using median of difference from LiDAR and standard deviation of that difference 27

16 Model to LiDAR correlation for up and down valley cases 28

17 Median wind power density for up and down valley cases 29

18 Model to LiDAR profile correlation for unstable, neutral, and stable stability conditions at 80 m height 31

19 Median wind power density for unstable, neutral, and stable stability conditions . 32

20 Model to LiDAR profile correlation at 80 m height for four different speed classes based off 10 m height AWS wind speed: a) 0-5.5 m/s, b) 5.5-7.9 m/s, c) 7.9-10.7 m/s, d) 10.7+ m/s 33

21 Median wind power density for four different speed classes based off 10 m height AWS wind speed: a) 0-5.5 m/s, b) 5.5-7.9 m/s, c) 7.9-10.7 m/s, d) 10.7+ m/s . . . 35

List of Tables

1 (Wieringa, 1986) Estimated roughness length parameters for the boundary layer, experimentally derived under neutral stratification 7

2 Checks for data quality applied during pre-processing 17

3 Profiling models used 17

4 Dependencies of each model. Measurement dependency is marked with 'x' and intermediate dependency is marked with 'o' 18

5 Cases for evaluating model usability 20

6 Slope for 10 m vs 2 m height windspeed in fig. 9 23

7 Statistical values for all study case when comparing model to LiDAR profiles at 80 m height 28

8 Statistical values for up valley flow when comparing model to LiDAR profiles at 80 m height 29

9 Statistical values for down valley flow when comparing model to LiDAR profiles at 80 m height 29

10 Statistical values for unstable conditions when comparing model to LiDAR profiles at 80 m height 30

11 Statistical values for neutral conditions when comparing model to LiDAR profiles at 80 m height 30

12 Statistical values for stable conditions when comparing model to LiDAR profiles at 80 m height 31

13 Statistical values for 0-5.5 m/s wind speed when comparing model to LiDAR profiles at 80 m height 33

14 Statistical values for 5.5-7.9 m/s wind speed when comparing model to LiDAR profiles at 80 m height 33

15 Statistical values for 7.9-10.7 m/s wind speed when comparing model to LiDAR profiles at 80 m height 34

16 Statistical values for 10.7+ m/s wind speeds when comparing model to LiDAR profiles at 80 m height 34

Abbreviations and List of Variables

Abbreviations

AWS	Automatic Weather Station
CNR	Carrier-to-Noise Ratio
DBS	Doppler Beam Swinging
IEC	International Electrotechnical Commission
IQR	Interquartile Range Filter
LiDAR	Light Detection and Ranging
NPI	Norwegian Polar Institute
RHI	Range Height Indicator
UNIS	The University Center on Svalbard
WMO	World Meteorological Organization

List of Variables

Variable	Units	Description
u	m/s	wind speed at height z (subs $1, 2, r$)
z	m	height (subs $1, 2, r$
z_T	m	height of temperature measurement(s)
T_0	K	reference temperature
u_*	m/s	friction velocity
Δu	m/s	difference in wind speed between u_1 and u_2
z_0	m	roughness length
θ	K	potential temperature
Ri		Richardson's number
g	m/s^2	gravity constant = 9.81
L	m	Monin-Obukhov length
ϕ_m		stability parameter, non-dimensional wind shear
κ		von Kárman constant = 0.4
α		Hellmann exponent

1 Introduction

Renewable energy is ever increasing in the modern energy grid with a growing portion from wind. Global wind production in 2021 was 823 GW out of 8013 GW, only 10.3%, according to the US Energy Information Administration. Arctic communities are still largely dependent on fossil fuels, with up to 79% entirely dependent on diesel (de Witt et al., 2021). Therein lies irony as Arctic regions experience the effects of climate change up to 7 times greater than worldwide with an average warming across the Arctic region 4 times higher than over the globe (Rantanen et al., 2022). There is also the issue of complicated logistics and substantial cost of fossil fuels for remote Arctic regions (de Witt et al., 2021). As such, renewable energy is being explored for Arctic use including solar, geothermal, hydroelectric, and wind. Wind energy is desirable as there is high energy potential in the Arctic. Several key tools are necessary to facilitate wind energy development in these areas.

Wind turbine installation requires knowledge of vertical profiles of horizontal wind speed. Knowing the wind speed at the hub height is necessary to estimate annual energy production. Knowing the entire profile allows for better estimates of wind loading throughout the structure and blades, especially as turbines reach hub heights of 100 m and beyond (Dimitrov et al., 2017). Further study of the wind profile provides insight to turbulence at the site. The wind turbulence model used and input properties such as length scale, dissipation, and anisotropy significantly impact the wind loading on wind turbines.

Wind profiles can be studied using LiDAR data. However, LiDAR experiments are expensive to carry out. To cut costs and rapidly evaluate potential wind energy generation sites, extrapolation methods are applied to pre-existing wind speed measurements taken at a standard 10m height. Such methods are understood for developed wind energy production regions such as the Midwest plains in the USA (Newman & Klein, 2014). Further, the accuracy of models has a high impact on predictions given the wind speed cube law. While many tools exist, the basic extrapolation methods used for wind profiling are vital and must be well understood (Murthy & Rahi, 2017). These methods are much less explored for remote regions such as those found throughout the High Arctic. Some models contain coefficients for which the best value is still being discussed and contain assumptions of the boundary layer which do not always mimic the natural world. Even if the extrapolation is well tuned for a particular hub height, the full wind profile is not necessarily captured accurately.

Further, the high Arctic in particular hosts unique characteristics and is less understood. The polar noon/midnight cycle produces a unique boundary layer which is still being studied. Further, the surface varies much annually due to shifting snow-pack and an active permafrost layer which adds another variable to the local climate system. Known models are tested in moderate, lower latitude climates, by comparison, which have a typical diurnal cycle and less annual ground variability. These differences leave open the question of validity for existing wind profile extrapolation methods in Arctic regions. Wind profiles constructed from LiDAR data can be used to test and evaluate such methods.

This project aims to construct and compare vertical profiles of horizontal wind speed from wind speed measurements taken in the Adventdalen region on Svalbard during the summer of 2022 using an automatic weather station (AWS) and a LiDAR campaign. The LiDAR constructed profiles are a baseline for comparison while the AWS data is used solely to construct model profiles. The goal being to evaluate the performance of several models using typical 2 m and 10 m height AWS data. The impact being that if any of the models are good enough, AWS stations can be used for wind energy forecasting. In turn this would pave the way for a more cost effective alternative to wind mast and LiDAR installations for evaluating wind resources in remote Arctic communities.

2 Background

2.1 Arctic Energy Resources and Development

553 remote Arctic communities were surveyed for their energy use and resources by de Witt et al. (2021). It was found that while most were dependent on diesel, 54% of the power generated was from diesel and 44% was from hydropower. This reflects the impact of higher upfront cost and minimum generation per site from hydro than from diesel. Less than 3% of generation is from wind and other renewables combined. They also note the distinction between dispatchable (e.g. diesel, batteries) and non-dispatchable (e.g. wind, solar) energy sources. A community may exclusively use dispatachable sources as they can quickly adjust to demand but non-dispatchable sources always require some form of dispatachable source for generation lulls. Nonetheless, such hybrid systems significantly reduce emissions and on-going cost for their community, albeit at higher upfront cost.

Diesel energy generation is well established in Arctic communities. And while a developed network exists for their servicing and refueling, the logistical risks still remain. Communities are also highly vulnerable to market shifts in price, supply, and demand with little possible alternative.

Hydropower is a good alternative for larger communities and in fact somewhat common, with 7 out of the 10 largest communities using it (de Witt et al., 2021). Hydropower has high upfront cost, especially for smaller plants but guarantees a low cost of electricity in the long term with minimal dependence on external markets. Unfortunately, hydropower has a high upfront cost and requires either substantial river flow or damming which has a significant environmental impact.

Solar energy generation is being used in the Arctic as well on very small scales e.g. 10 kW, with most installations being private and for home energy supplementation or remote cabins. Testing is already being done for larger scale expansion in Longyearbyen, Svalbard (Lokalsamfunnsplan, 2023). While some generation is possible, the odds are stacked against larger scale use. Photovoltaic cells have a high energy and negative environmental cost of manufacturing. They also take up significant ground area compared to other energy generation methods when it is not possible to install panels on buildings. Lastly, snow coverage is a concern still being investigated.

Wind power installations are already being tested in the Arctic and have good potential. Canada has an ongoing program, "A Cold Wind Blows: Seeking Smaller, Ruggedized Wind Turbines for the Arctic", which is funding the development of turbines for high Arctic environments. Wind turbines face challenges of icing and cold temperature material properties leading to shorter fatigue life (Wallenius & Lehtomäki, 2015). There are also challenges related to installation on permafrost and complex logistics (de Witt et al., 2021). Solutions to the technical challenges are in development and some are already in use. However, much further study and testing is still necessary to lower cost and optimize wind turbine design for the high Arctic.

Arctic regions suffer a much higher cost of power outage and risk to the community than in temperate regions (de Witt et al., 2021). As such, redundancy is critical to energy system design. Diesel still presents itself as the ideal solution in this scenario when compared to batteries. Even under successful implementation and operation, the challenges above make for a high economic cost to households for electricity with the average in Arctic communities being 30 USD ¢/kWh and up to 181 USD ¢/kWh. Given the high economic cost, cheaper methods of energy generation are needed. Further, high cost of renewable energy severely limits the ability of Arctic communities to make such a transition. Cheaper site evaluation methods can reduce this cost.

2.2 Use of Automatic Weather Station Data

Automatic weather stations (AWS) record wind speed and temperature measurements around 2 m and 10 m height. Such data is used for weather reporting and forecasting for local communities as well as scientific research. Given AWS broad use, they are relatively common providing a vast data-set which may be used for wind energy siting. More direct measurements using wind masts or LiDAR are preferred given their accuracy. However, this is both expensive and time consuming as at least 1 year of data is necessary to evaluate a site, preferably 3-10 yr.

Sjöblom (2014) investigates observation methods for heat flux using a field campaign in Adventdalen, the same site used in this project. Methods using common AWS instrumentation were compared against methods requiring more sophisticated instrumentation. Two of the methods required calculation of the roughness length. Roughness length was found to be sensitive to the wind direction and sensitive to wind speed making calculation difficult. As expected, the methods required more sophisticated instrumentation had a better fit to the most direct method than the method using common AWS instrumentation. The methods were found to also be highly sensitive to the roughness length meaning heat flux calculations are highly sensitive to data quality and therefore the instrumentation used.

Given the demonstrated high sensitivity to data quality, care is taken in handling AWS data following the approach taken by Sjöblom (2014). She also provides a good comparison for checking methods and results as the data collection was from the same site as used in this project. As Sjöblom (2014) emphasizes, the climate is very local in Adventdalen due to the breadth of contributing factors. This means the context of this project must be well-defined to produce good results. In this project, the roughness length is a key value. Caution must be used in calculating it for this region. Lastly, the empirical models used require some level of decision on the coefficients to use. Sjöblom's approach here provides values for those coefficients and validates their use.

2.3 Boundary Layer Wind Speed Profiles

The boundary layer is defined as the bottom the lowest part of the atmosphere where the air is directly affected by the ground. Stull (2009) further constrains the definition to where the effects of the surface are seen at periods of 1 hr or less. The boundary layer thickness varies significantly. It can be less than 100 m to more than 3000 m. The surface layer is roughly the bottom 10% of the boundary layer. Wind speed in the surface layer can studied using LiDAR or a wind mast, for example. Both of the instrumentations are expensive to install. However, given AWS measurements at only 2 m and 10 m height, extrapolation methods can be applied to determine the wind speed at wind turbine hub height.

Typically, a designer will use one of several wind profile extrapolation methods to determine the wind profile at the site. Data comes from metocean databases built from on site-measurements or hindcast data. Wind masts and LiDAR stations can also be installed to create a broader dataset. The extrapolation methods typically used are empirically derived and as such have none to poor relation to analytical models but can make good estimates of hub height wind speed (Gualtieri & Secci, 2014; Peterson & Hennessey, 1978). Analytically derived models do exist and are used in meteorological contexts (Lopez-Villalobos et al., 2022; Newman & Klein, 2014).

The boundary layer has not yet been explored significantly in the Arctic. Offshore wind development has seen a surge in growth over the past decade. Wind energy has been under development for several decades longer leading to a noticeable knowledge gap between on and offshore wind modeling. Given the close proximity of Arctic communities to the ocean, the knowledge gap can provide insight to the Arctic wind energy knowledge gap. Kalvig et al. (2014) found that constant roughness length could be a poor assumption as environmental factors such as snowfall, drifting, and ground ice build up and vary throughout the year. Also, for Arctic regions such as Svalbard, terrain features vary significantly over relatively short distances including mountains, plateaus, valleys, and glaciers. This points to a need for evaluating these and other models within the Arctic context.

2.3.1 Power Law

The power law is an empirical derivation which requires the assumption of neutral stability. The power law is used in the IEC 61400-3 standard (*Design requirements for offshore wind turbines*, 2019) with shear exponent $\alpha = 1/7$ shown in (1). u_z is the wind speed at height z, u_r is the wind speed at the reference height z_r, and α is the shear exponent factor also known as Hellmann exponent. Peterson and Hennessey (1978) validates the traditional use of $\alpha = 1/7$ in smooth terrain. The basic power law assumes a constant shear exponent. However, this varies with height. (2) can be used to calculate the shear exponent based on roughness length z_0 and wind speed height as found by Sedefian (1980). This improves the power law by taking into consideration two key pieces of information.

z_0 is the roughness length which is defined as the equivalent height at which the

wind speed becomes zero assuming no ground obstacles. Typical values are shown in table 1. In the Sedefian model, the shear exponent is calculated at each height due to it's dependence on height z. Surface roughness can also be calculated for an area using (3) by relating the known wind speed at 2 m and 10 m heights. Roughness length remains consistent as long as the ground conditions remain consistent. While snow is present throughout winter in Adventdalen and varies annually, the ground conditions were consistent throughout the the summer campaign. The calculated roughness length is 0.004 m using the median roughness calculated at neutral conditions (fig 1). Median is chosen over mean as to minimize the effect of several outliers differing on an order of magnitude greater. For comparison, Sjöblom (2014) calculated the roughness length to be 0.0035 m but also found 0.0005 m to provide for a better fit, albeit nonphysical. Also, the table of values compiled by Wieringa (1986) gives 0.005 for comparable terrain which furhter validates.

$$u_z = u_r(z/z_r)^{\alpha} \tag{1}$$

$$\alpha = \ln^{-1}(z/z_0) \tag{2}$$

$$z_0 = e^{\frac{u_2 \ln(z_1) - u_1 \ln(z_2)}{u_2 - u_1}} \tag{3}$$

Table 1: (Wieringa, 1986) Estimated roughness length parameters for the boundary layer, experimentally derived under neutral stratification

Class	Description	$z_0(m)$
1	Sea - Open sea, fetch at least 5 km	0.0002
2	Smooth - Mud flats, snow: little vegetation, no obstacles	0.005
3	Open - Flat terrain; grass, few isolated obstacles	0.03
4	Roughly open - Low crops; occasional large obstacles	0.10
5	Rough - High crops; scattered obstacles	0.25
6	Very rough - Orchards, bushes; numerous obstacles	0.5
7	Closed - Regular large obstacle coverage; (suburb, forest)	1.0
8	Chaotic - City centre with high- and low-rise buildings	> 2

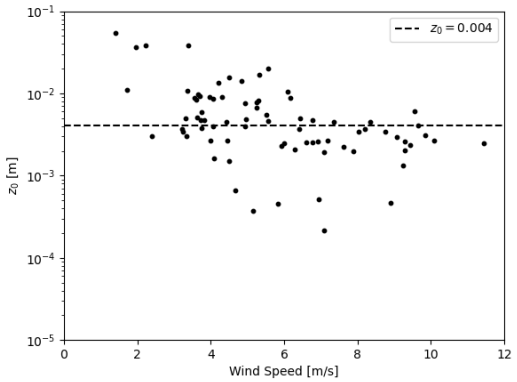

Figure 1: Roughness length calculated near neutral values using AWS data at 2 m and 10 m heights.

2.3.2 Log Law

Typically, wind speed increases with height as friction dampens air flow to zero at the ground. With increasing height, air pressure decreases and air flow simultaneously increases as a response following pressure-velocity relation in Bernoulli's equation. The log law is commonly used to describe the surface layer and derived both empirically and analytically Stull (2009). Under statically stable conditions, the wind speed follows a logarithmic relation with height which is the basis for the empirical derivation. The derivation is further supported by the non-dimensional relationship of mean wind speed to friction velocity $\frac{\overline{U}}{u_*}$ and height with roughness length z/z_0. Analytically, the log law is derived from integrating the momentum flux term in the equations of motion for wind. Momentum flux is near constant in the surface layer by definition which simplifies the equation. Integrating over the height from roughness length produces the log law (4). u_* is the friction velocity and requires flux measurements of wind in the cardinal and vertical directions. k is the von Kárman constant; found to be 0.4 (Högström, 1996). z_r is the height at which u_r is found and z_0 is the roughness length.

Flux measurements require high speed capture which is not possible with the AWS instrumentation. However, since the vertical profile of horizontal wind speed follows a logarithmic profile, any two points along the profile can be related as shown in (5) by dividing (4) at two heights. This provides a more simple method which is able to use AWS data.

$$u_r = \frac{u_*}{k} ln(z_r/z_0) \tag{4}$$

$$u_2 = u_1 \frac{ln(z_2/z_0)}{ln(z_1/z_0)} \tag{5}$$

2.3.3 Stability Considerations

In both power law models and the basic log law, stability conditions are not accounted for which means power performance is not adequately represented. Kalvig et al. (2014) note that power estimations improve significantly if stability is taken into account. Stability also needs to be accounted for in these models for wind loading. By improving these models using simple correction terms, turbines can be better design for long term fatigue on rotors. A stability term is added, giving (6). ϕ_m is the integrated corrective function also known as the non-dimensional wind speed shear term (7). L is the Monin-Obukov length.

$$u_2 = u_1 \frac{\ln(z_2/z_0) - \phi_m}{\ln(z_1/z_0) - \phi_m} \tag{6}$$

$$\phi_m = \left\{ \begin{array}{ll} 2\ln(\frac{1+x}{2}) + \ln(\frac{1+x}{2}) - 2tan^{-1}(x) + \frac{\pi}{2}, & \text{for } \frac{z}{L} < 0 \\ \quad x = (1 - 19\frac{z}{L})^{\frac{1}{4}} & \\ -5.3\frac{z}{L}, & \text{for } \frac{z}{L} > 0 \\ 0, & \text{for } \frac{z}{L} = 0 \end{array} \right\} \tag{7}$$

Within the surface layer, L is constant which allows for the stability term $\frac{z}{L}$ to be recalculated at every height.

2.4 Use of LiDAR Data

Given the high cost of wind mast installation and already available LiDAR data, LiDAR is used as a baseline for evaluating the models. LiDAR has its own set of challenges, however, regarding data availability and quality. (Beck & Kühn, 2017) investigates methods of filtering LiDAR scans to maximize the quality while taking an acceptable decrease in data availability. Some methods produce accurate data but at the cost of significantly reducing the number of data-points which are usable. The dynamic data filters simultaneously maintain good accuracy and ok data availability and are computationally more advanced and expensive than traditional methods.

The first method is the most common. Carrier-to-noise ratios (CNR) are used as a data threshold. This varies from manufacture to manufacture but as an example, all values with a CNR value less than -24 dB are removed from the dataset. In addition to significant data being lost, CNR values tend to increase with range which severely limits the area of data coverage. A dynamic filter will account for the range in the cutoff or use methods independent of the CNR value altogether. In this case, the filter aims to determine mean velocity which means the resolution of the scan is significantly reduced. That is suitable for the applications of this paper but not necessarily suitable for turbulence studies.

Several other filters are compared to the designed dynamic filters. A static two standard deviation filter removes values based on a set standard deviation from the mean. This method has potentially unpredictable performance as high noise data might be under-filtered and low noise data might be over-filtered and in any case can have significant data loss. This method also assumes specific data distribution which may not be the case. As a similar approach, the interquartile range filter (IQR) has a hard cutoff of the upper and lower 25% of datapoints. This makes no assumptions regarding data distribution. The IQR filter produces middle tier quality data in their analysis with high availability (93.5%) (Beck & Kühn, 2017). While more complex filters are evaluated, including two proposed by the authors which perform even better than the IQR, they are found to be more complex than necessary for this project.

Beck and Kühn (2017) conclude that wind speed errors do not fit a normal distribution explaining the limiting effectiveness of standard deviation filters. While a two standard deviation filter maintained 96% data availability, it had middle tier accuracy. The CNR threshold is fast, but significantly lowers the data availability. While the authors conclude that their proposed dynamic filter accuracy is worth the loss in data availability, this is not acceptable for this project as data availability is already a significant challenge.

2.5 Summary and Project Goal

Arctic communities tend to have limited resources and renewable energy installations are expensive, time consuming, and logistically complex. They require high upfront costs for site evaluation typically using expensive tools such as computer simulations, wind masts, LiDAR, or a mix of the above. The manufacturing and logistics of installation also have high cost. Most Arctic communities are dependent

on expensive fossil fuel resources for electricity generation, further inhibiting the ability to make an energy transition. (de Witt et al., 2021) shows that Arctic communities have established power with a need for an energy transition. While the transition has many challenges, the potential is great. Hydropower, wind, and solar present renewable options across a wide breadth of energy and cost scales. For it's abundance and wide scalability, wind is further investigated in this project. While there are economic aspects to be considered, that is beyond the scope of this project.

(Beck & Kühn, 2017) provides a method of handling LiDAR data to ensure quality. (Sjöblom, 2014) provides a method of handling AWS data, the foundational first steps for calculating the models, and some direct comparisons. (Newman & Klein, 2014) provides a solid example of model analysis as well as a baseline comparison for model performance. While set in a different context, the analysis used is a key reference for this project.

This project focuses on the site evaluation step of wind energy installation, specifically the wind speed extrapolation methods used. AWS data may be usable for site evaluation, providing a vastly cheaper and less time consuming option. AWS, if not already installed, are relatively cheap and provide benefits to the local community far beyond energy prediction. This project aims to evaluate existing extrapolation methods of vertical profiles of horizontal wind speed for their strengths and weaknesses in an Arctic context. The models evaluated are all constructed solely from AWS data to generate predictions of wind speeds at turbine hub-height. The baseline profiles are constructed from LiDAR RHI scans.

3 Method

3.1 Location

The data used in this project was collected as part of another project for Matthias Henkies. A LiDAR station was setup near Longyearbyen at the old UNIS aurora observatory in Adventdalen on Spitsbergen. The location is shown in figure 2. Spitsbergen is an island within the Svalbard archipelago located north of Norway from 74°to 81° N and 10° to 35° E. It is characterised by deep fjords, 60% coverage by glacier, and broad valleys shaping a highly localized climate. The AWS coordinates are 78° 12' 10" N, 15° 49' 41" E and 15 m altitude above sea level. The LiDAR was placed approximately 100 m WNW of the AWS. The temperature over the course

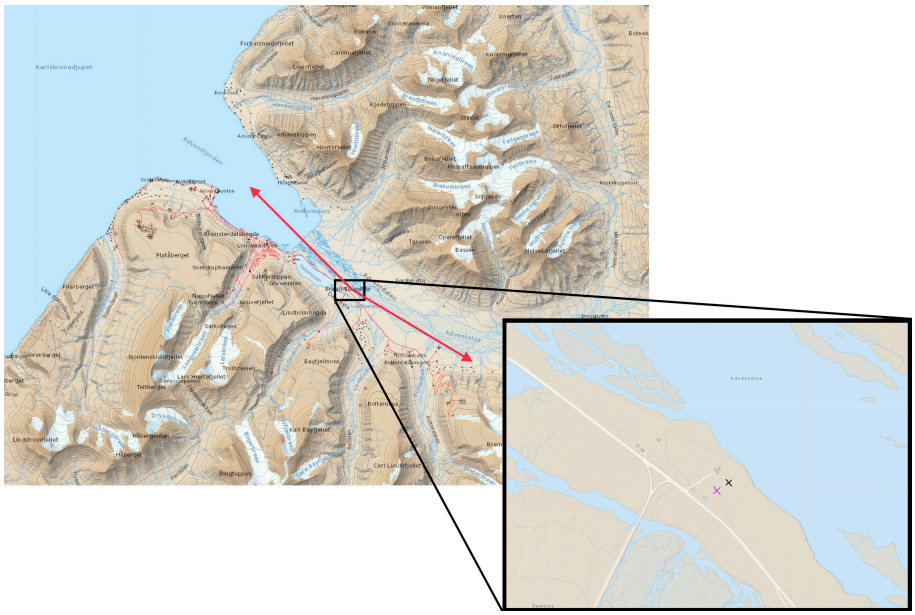

Figure 2: Location of the LiDAR (purple) and AWS (black). The red arrows indicate the down and up valley scan headings and reach. (Norwegian Polar Institute, n.d.)

of the campaign was an average of 8.3°C with a high of 16.6°C and a low of 1.3°C at 10 m height. The average wind speed was 5.1 m/s with a high of 14.6 m/s and a low of 0.0 m/s at 10 m height.

3.2 LiDAR

LiDAR at its most basic level works by measuring the Doppler shift of aerosols in the air. A laser beam is emitted at an azimuth and elevation. The reflected light from aerosols is measured for distance and Doppler shift along the line of sight. The Doppler shift is used to locally calculate the radial wind speed away from the LiDAR station at the azimuth and heading. This data is then filtered and processed to create vertical profiles of horizontal wind speed. These profiles are then used as a benchmark for wind speed extrapolation methods.

3.2.1 Data-collection

The LiDAR station collects data through several routines. Range height indicator (RHI) mode repeats the scan through the azimuth from 0° to 90° in 1° intervals to produce a slice of the radial wind speed up and down the valley. Doppler beam swinging (DBS) takes measurements directly overhead in pairs aligned with north-south and east-west headings producing vertical profiles of horizontal wind speed and direction. The LiDAR maximum range is 7100 m and the minimum is 100 m with a range gate of 50 m. While DBS scans are a more direct measurement of the wind speed profile, they require the instrument to be directly beneath the site of the desired profile which is not always possible and measure only from the minimum range upwards.

RHI scans can provide wind speed profile data throughout the investigated heights through processing which is detailed below. DBS scans have a minimum measurement height of 100m which is too high for boundary layer modeling. Therefore, RHI scans are used for producing the vertical profiles of horizontal speed used in profiling validation while DBS scans are used validate RHI data processing above 100m. In addition, a nearby automatic weather station is used to validate processing at 10m height.

The LiDAR unit collected data from 04-07-2022 10:05 until 23-08-2022 15:38. RHI scans were taken continuously between xx:10 and xx:50 every hour with a full scan period of approximately 3 minutes. DBS scans were taken at varying intervals resulting in a calculated direction and speed around every 5 seconds.

3.2.2 Processing

Several processing steps are applied to the RHI scans before vertical profiles are created (fig 3). Portions of the scan are removed for too high measurement angle. The carrier to noise ratio (CNR) is used as a standard method of filtering poor quality datapoints. Then corrections are made for horizontal windspeed. An interquartile filter further removes poor quality datapoints. Lastly, the vertical profiles of horizontal wind speed are constructed. Above 30°, the LiDAR scans consist of an

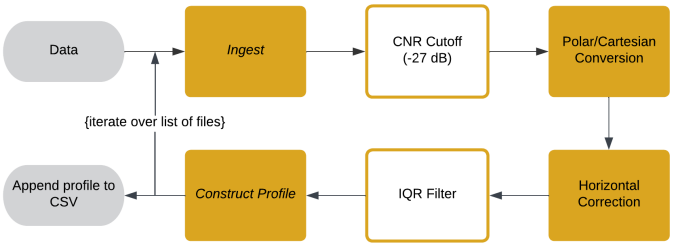

Figure 3: LiDAR processing steps. Solid gray blocks are inputs/outputs. Solid gold blocks are data handling steps. Gold bordered blocks are filters.

increasingly strong vertical speed component of $u_{vertical} > 0.5u_r$ where u_r is the measured radial speed component. To use more direct measurements of horizontal wind speed, 30° is used as the cutoff angle. Also, at steeper angles there is a higher chance of measuring the speed precipitating particles.

The carrier to noise ratio (CNR) is a calculation of the backscatter of the return signal. Typically, a manufacture recommended CNR value or one selected based on prior studies from -22 dB through -27 dB is used to eliminate data points below that threshold. Beck and Kühn (2017) found -24 dB to be most appropriate with their data. Based on CNR vs radial speed plots taken over the dataset, a threshold of -27 dB is set. The lower threshold is also supported by an increase in speed variance caused by lower aerosol content in the air (Piironen & Eloranta, 1995). A 30 year study found lower aerosol counts in the Ny-Ålesund area than the rest of Europe (Platt et al., 2022). It is then inferred that similarly lower aerosol content is in Adventdalen given its' relative proximity to Ny-Ålesund. Ny-Ålesund lies only 110 km NW of Longyearbyen and Adventdalen.

In an example plot (fig 4), The average of the more dense band of noise is around -33 dB with upper and lower limits of noise around -27 dB and -35 dB, respectively. From 0 to -8 m/s speed there is a high density region of data points. Based on (Beck & Kühn, 2017), this is likely a set of otherwise quality data therefore a threshold of -27 dB is used.

Following LiDAR processing, the data is merged and pre-processed with AWS data

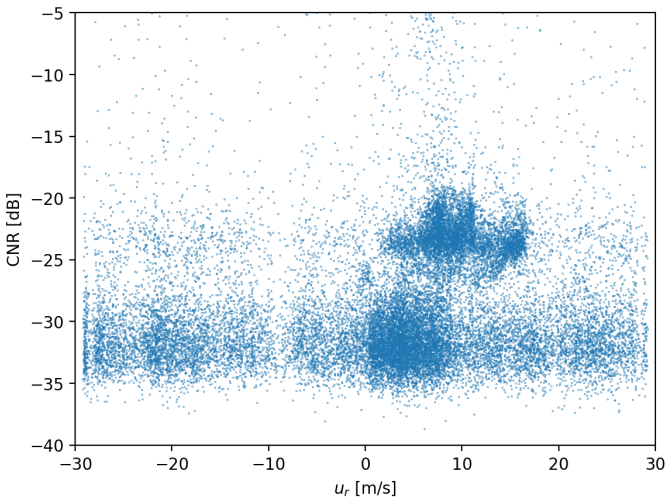

Figure 4: CNR and radial speed on 2022-07-15 19:18:02 - 19:19:31 UTC

to create a set of suitable data points (fig 6). Since the LiDAR RHI scan measures radial windspeed, (8) is used to convert the measurements to the standard, horizontal wind speed. θ is the elevation angle of the scan in degrees. Since radial wind speed decreases with increasing elevation angle due to less direct measurement of the horizontal wind, the interquartile filter is applied after the horizontal wind speed correction. This prevents filter bias towards removing the highest or lowest elevation angle points.

$$\frac{u_{radial}}{u_{horizontal}} = cos(\theta) \tag{8}$$

Since the CNR cutoff is lower than typically used, some poor quality data points still get through. As such, an interquartile filter is used to remove these points shown in (9). IQR is the middle 50% quartile range and u_h is the horizontal wind speed with

$u_{h,25}$ being the lower quartile and $u_{h,75}$ being the upper quartile. This approach is selected based off (Beck & Kühn, 2017) since it has high data availability (93.5% in their case), good quality, and is easy to use. Ease of use is important to this project as the LiDAR profiles themselves are not the focus. This filter applied to each scan separately.

$$u_{h,25} - 1.5IQR < u_h > u_{h,57} + 1.5IQR \tag{9}$$

3.2.3 LiDAR Wind Speed Profile Construction

Since the wind profile is being constructed over only a fraction of the area recorded, the data is cropped. This removes the influence of missing data and artifacts outside the area of interest. As such, a total area for the wind profile construction, from 150 m to 1000 m distance and 0 m to 150 m height is designated. Following filtering,

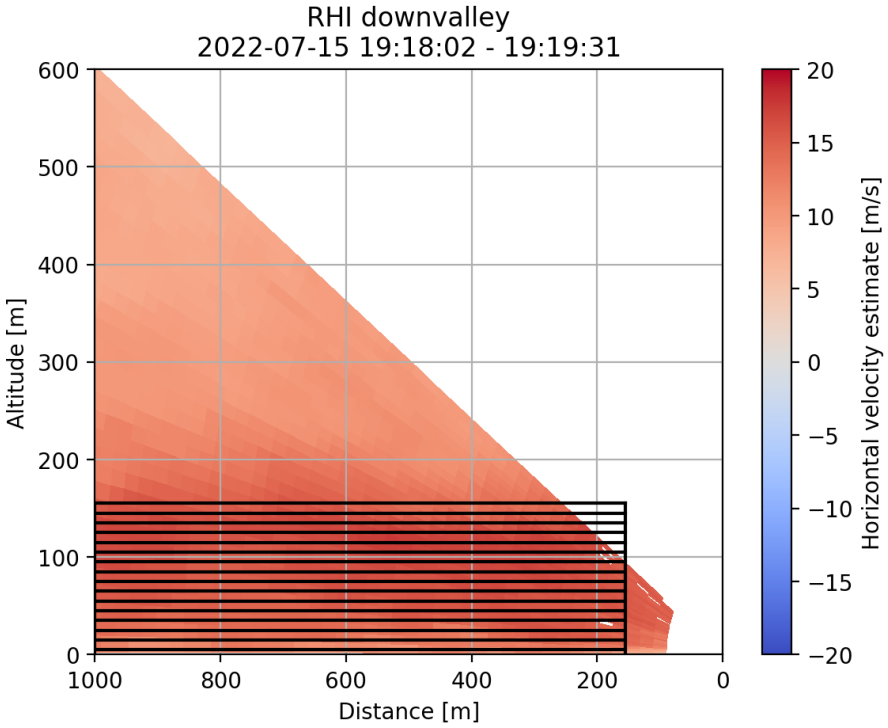

Figure 5: Selection slices of an example RHI scan for calculating median vertical profile of horizontal wind speed. Taken on 2022-07-15 19:18:02 - 19:19:31 UTC

median wind speed is calculated over a designated area. An example sketch of the area used is shown in (fig 5). All points within each horizontal slice are selected and then the median is taken. The area defined above is sliced into horizontal boxes based on a selected resolution. The median is placed at an altitude of the midpoint of the slice. For example, for 10 m height the points from 5 m to 15 m height are used. Median is chosen over mean since high speed outliers may still pass through the above filters and significantly influence the average in low to medium wind speed scenarios. A minimum of 50 datapoints within the 150 m by 1000 m region is required to construct a profile. A minimum per slice is not set as incomplete profiles are filtered out later on.

Each box is a very small subset of the total possible area covered by RHI scans in terms of area but still contains substantial datapoints. A shorter box has the advantage of reducing the influence of topography and coastline. Often, little to no quality points are reported beyond 2000 m distance due to high noise as can be seen in the figure. A longer length for the box reduces turbulence effects although lengths greater than 100 m are sufficient for removing any small scale turbulence effects. Placing the starting point at a further distance from the instrument has the advantage of reducing the reach of upper slices into the above 30° cropped region which would reduce the effective number of sampled points. Lastly, the maximum height of the box is based on the height of boundary layer horizontal wind speed profile to be evaluated, 200 m.

3.3 Automatic Weather Station

Automatic weather stations (AWS) take common measurements to more easily make direct comparisons between sites. The World Meteorological Organization (WMO) has a standard for taking measurements with flexibility for some criteria outlined in "Generic Automatic Weather Station (AWS) Tender Specifications)". This standard is not always followed exactly. Nonetheless, temperature measurements are to be taken somewhere between 1.25 m and 2 m and wind measurements at 10 m height. Using these common measurements is key to this project as favorable methods can then be used at similar sites around the world. While masts higher than 10 m are certainly possible and do exist, the difficulty in setup and engineering rapidly increases with height.

The AWS in Adventdalen has a breadth of instrumentation which in sum goes beyond the WMO standard. Used in this project are wind speed and direction and temperature, all with slow-response measurements at 1 Hz. The station is maintained by UNIS. For wind speed and direction at both heights, a 05103-34 Alpine Wind Monitor made by R.M. Young Co., Traverse, Mi, USA is used. It has an accuracy of ± 0.3 m/s or 1%, whichever is greater. Temperature measurements are taken using a naturally ventilated 41342 Platinum Temperature Probe made by R.M. Young Co., Traverse, Mi, USA. It has an accuracy of ± 0.1 deg C.

The temperature is taken at 2 m and 9 m heights and wind speed and wind direction are taken at 2 m and 10 m. The 9 m temperature measurement is below 10 m for geometry considerations of the structure. Temperature is reported every 1 second as an instantaneous value, the average over the past 1 second, standard deviation and expected error. Wind speed and direction are reported every 1 second as the averages over the past 1 second and the standard deviation. The data was re-sampled to 10 minutes average before being used further on.

3.4 Pre-processing

Before profiles are constructed, several routines are followed to maintain data quality and validity in comparison (fig 6). The steps use a mix of either or both the

AWS and the LiDAR RHI based profile and DBS scan datasets so the data path of each is also shown. First, the datasets are re-sampled and synced. Then corrections are made for wind speed and direction. Filters are then applied to keep only data under conditions specific to this project and a last filter to check the impact of specific conditions on the models. Lastly, the models are constructed from the AWS data and compared to the LiDAR RHI based profiles. Given the RHI scan

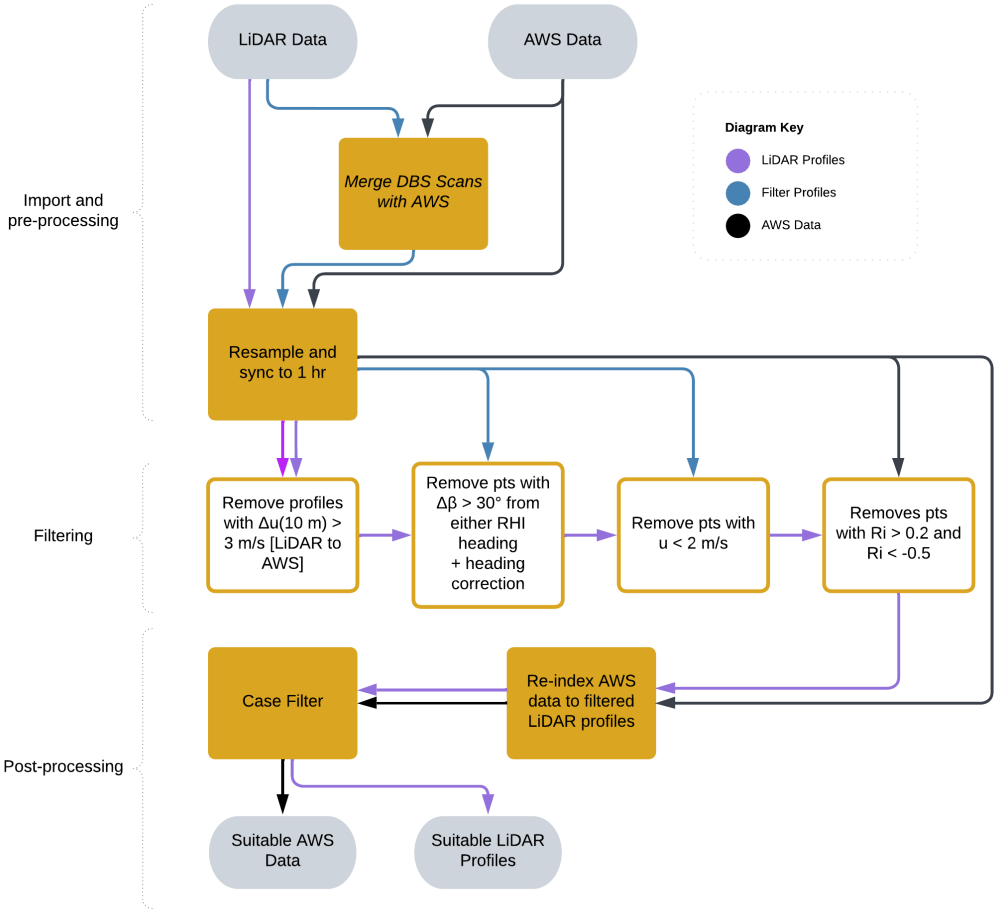

Figure 6: LiDAR and AWS data pre-processing steps. Colored paths indicated the use of specific datasets. Solid gray blocks are inputs/outputs. Solid gold blocks are data handling steps. Gold bordered blocks are filters.

contained a 20 minutes gap every hour, the LiDAR and AWS data were re-sampled to 1 hour period, closed and labeled on the right end on the hour. The datasets were then synced providing a baseline for making corrections and comparisons between parallel datapoints.

Several checks were applied for quality control of the data going into profiles, shown in table 2. The LiDAR at 10 m height does not always match the AWS at 10 m. The causes for this discrepancy and use of various filtering methods on RHI scans is beyond the scope of this project so all data points with a difference greater than 3 m/s are then removed. Since the wind direction is known only at 10 m (AWS) and 100+ m (DBS), these heights are used for the wind speed and direction checks. These heights are sufficient for this project as wind direction profiles are outside the scope and only used for quality control. After the wind speed and direction checks, the wind speed is corrected at each height using the wind direction and (10). β_{wind}

Table 2: Checks for data quality applied during pre-processing

Check	Description
$\Delta u > 3$m/s	Difference in wind speed measured by AWS from LiDAR profile at 10 m height.
$u > 2m/s$	Minimum wind speed. Below this, electrical power cannot be generated. The speed is also too low to create an accurate profile as the error component dominates the sensor reported values.
$\Delta\beta < 30°$	Similar to the 30° cutoff, wind speed is poorly measured when the direction is more than 30° from the RHI scan heading.
$-0.5 < \mathrm{Ri} < 0.2$	Stability model is not valid outside these condition.

is the wind direction and β_{RHI} is the LiDAR RHI scan heading.

$$u_{corrected} = u/cos(\beta_{wind} - \beta_{RHI}) \tag{10}$$

3.5 Model Profiles Construction

There are two basic profiling methods commonly used, the power law and the log law. Two variations on each of those methods are studied. In summary, they are shown in table 3. The variable dependencies of each model are shown in table 4. Dependency refers to required measurements and intermediate dependency refers to quantities which are found during intermediate steps. The profiles constructed prior from the LiDAR scans are used solely as a benchmark. The investigated profiles are modeled entirely using data from the AWS in Adventdalen. The wind speed direction and filtering used above are used only for making apples to apples comparisons between the LiDAR and model profiles. If these models are applied, only the speed at AWS heights would be used for filtering. The wind direction, while necessary for evaluating shear and torque on the turbine, would not be used for filtering prior to modelling as the wind speed measurements are accurate in all directions.

Table 3: Profiling models used

Method	Short-hand	Variation	Equation
Power Law	IEC	IEC 61400 standard $\alpha = 1/7$	(2)
Power Law	Sedefian	calculated shear exponent based on roughness length and height	(1)
Log Law	log-neutral	basic form	(5)
Log Law	log-stability	with stability correction	(6)

Profiles are constructed using the four models from 10 m to 150 m heights at intervals of 10 m meters. 10 m is the AWS measurement height and 150 m is arbitrarily chosen as a height slightly above the likely maximum reach of wind turbines in coastal regions. This is based off publicly available data from The Norwegian Water Resources and Energy Directorate (NVE) on wind farms in northern Norway. The largest turbine has a hub height of 89.9 m with a rotor diameter of 115.4 m which means a maximum reach of 147.6 m. Turbines with higher hub height and maximum reach are commercially available so 150 m is selected to ensure coverage

Table 4: Dependencies of each model. Measurement dependency is marked with 'x' and intermediate dependency is marked with 'o'

Variable	IEC	Sedefian	log-neutral	log-stability
u_1	x	x	x	x
u_2		x	x	x
z_1	x	x	x	x
z_1		x	x	x
α	x	o		
z_0		x	x	x
T_1				x
T_2				x
Ri				o
L				o

in this analysis. 80 m height is focused further on as a common hub height seen in Northern Norway.

There is a difference in the AWS to LiDAR 10 m height measurements ranging from -2 to 3 m/s. Since the difference in LiDAR vs AWS measurement methods is not being studied here and the use of LiDAR is to compare profile trends with increasing height, the difference in AWS and LiDAR measurement is added to the entire LiDAR profile (12). This eliminates the bias caused by difference in measurement methods while still modelling based solely off the AWS.

$$u_{\text{diff}} = u_{\text{AWS}}(10\text{m}) - u_{\text{LiDAR}}(10\text{m}) \tag{11}$$

$$u_{\text{LiDAR,corr}}(z) = u_{\text{LiDAR}}(z) + u_{\text{diff}} \tag{12}$$

3.5.1 Stability Considerations

The log-stability method requires stability to be considered. The thermal stability term is z/L. Another non-dimensional parameter, Richardson's number also indicates thermal stability. The z/L term is related to Ri using the bulk Richardson's number by (13) as suggested by Arya (2001). There are three ways of calculating the Richardson's number. The flux Richardson number requires turbulent conditions so it is not chosen. The gradient Richardson number requires knowledge of the temperature and wind speed gradients which are not available. The bulk Richardson number is simpler, using differences in discrete points in space and can be further simplified to using one discrete point using assumptions about temperature and wind speed gradient. In the case of the Adventdalen AWS, data is available for two discrete points as preferred. Sjöblom (2014) suggests that even with the assumptions made in using the bulk Richardson number for one discrete point, the bulk method is usable if care is taken in managing data quality. As such, the bulk method is chosen for this project.

The bulk Richardson number is calculated using (14). g is the gravitational acceleration constant 9.81 m/s^2. T_0 is the reference temperature commonly taken at

2 m height for AWS and in Kelvin. $\Delta\theta$ is the change in virtual potential temperature with height. However, due to prevailing dry air in Adventdalen, the potential temperature is used. Further, the virtual potential temperature which accounts for moisture content is not necessary as the moisture content has little effect on stability calculations in the context of wind energy (Van Wijk et al., 1990). Therefore the dry adiabatic lapse rate yielding (15) in C° is used to calculate the potential temperature at each point. Δz_T is the difference in height for the potential temperature measurements in m. For the AWS, these are 2 m and 9 m. Δu is the change in wind speed in m/s. Δz_u is the difference in wind speed measurement heights in m. For the AWS, these are 2 m and 10 m.

$$\frac{z}{L} = \left\{ \begin{array}{ll} Ri, & \text{for } Ri < 0 \\ \frac{Ri}{1-5Ri}, & \text{for } 0 < Ri < 0.2 \end{array} \right\} \tag{13}$$

$$Ri_B = \frac{g}{T_0} \frac{\Delta\theta/\Delta z_T}{(\Delta u/\Delta z_u)^2} \tag{14}$$

$$\Delta\theta = T_2 - T_1 + 0.0098(z_2 - z_1) \tag{15}$$

Since Ri=0 is very specific, neutral conditions were considered where $-0.025 < \text{Ri} < 0.025$ as used in Sjöblom (2014). Unstable conditions are $\text{Ri} \leq -0.025$ and stable conditions are then $0.025 \leq \text{Ri} < 0.2$. For $\text{Ri} \leq -0.5$ and $0.2 \leq \text{Ri}$, the data point is thrown out as the Ri to z/L relation is not valid.

3.6 Wind Energy Potential

The energy potential of wind is found using (16) known as the wind power cube law. ρ is the air density. A_r is the swept area of the rotor. u is the wind speed. C is the efficiency coefficient for the amount of energy which can be captured by the turbine. The theoretical limit for C was found by Albert Betz in 1919 to be 59.3%. The wind speed cube term is the focus for wind energy potential. The cube term means proper wind speed estimates are vital. For example, if the predicted wind speed is 10 m/s and the actual wind speed is 8 m/s, that is an overestimate of the energy generated by 156%. Therefore accurate models are vital for producing sufficient energy without significantly overestimating the project cost.

Since (16) requires knowledge of the wind turbine size, it can be rearranged to show the wind power density (17). The efficiency term can also be ignored since the predicted power density is being compared across different models for the same conditions.

$$E_{wind} = 0.5C\rho A_r u^3 \tag{16}$$

$$E/A = 0.5\rho u^3 \tag{17}$$

3.7 Study Cases

To better understand the useful conditions of these models, several cases are setup for limiting the context of their evaluation. Up valley vs down valley flow, stability conditions, and wind speed are considered. Typical stability is evaluated for each wind speed and flow direction case. The cases are outlined in table 5. Stability

follows the definitions above. Wind speed is divided using the Beaufort wind classes.

Up valley and down valley flow are compared due to the terrain difference. Down valley flow is influenced by smaller feeder valleys and gullies along Adventdalen. Up valley flow is influenced by Adventfjord. As such, there is expected differences in flow.

All models are limited by or dependent on stability conditions. As such, these are compared. Given the lower number of data points, three classes are used as opposed to five class typically found in literature such as Newman and Klein (2014), Motta et al. (2005), and Van Wijk et al. (1990). z/L is used in these cases for determining stability class since z/L is calculated using its relations to Ri. Therefore, it is acceptable to directly use Ri here for stability classification. The same divisions are used from earlier.

The wind speed is divided up following the Beaufort scale where the class 0-3 is 0-5.5 m/s, class 4 is 5.5-7.9 m/s, class 5 is 7.9-10.7 m/s, and class 6+ is $\geq$10.7 m/s. These are subjective divisions developed in 1805 by Sir Francis Beaufort of the British Royal Navy for better communicating and making notes of wind speed. While not necessarily used in discussions related to wind energy, they provide clear divisions for wind speed cases to be evaluated. The 0-3 classes are grouped as modern turbines have a typical cut-in wind speed of 3-4 m/s (Abolude & Zhou, 2017). Classes 6-12 are grouped based off of the common wind speeds in the Adventdalen area the summer campaign. The scale is applied to the AWS 10 m height data.

Case	Parameter
0	all conditions
1	down valley flow
2	up valley flow
3	unstable conditions ($-0.5 < \text{Ri} \leq -0.025$)
4	stable conditions ($0.025 \leq \text{Ri} < 0.2$)
5	neutral conditions ($-0.025 < \text{Ri} < 0.025$)
6	Beaufort 0-3 (0-5.5 m/s)
7	Beaufort 4 (5.5-7.9 m/s)
8	Beaufort 5 (7.9-10.7 m/s)
9	Beaufort 6-12 (>10.7 m/s)

Table 5: Cases for evaluating model usability

4 Results

The context of the 7 weeks campaign is presented first with basic description of the wind conditions and resultant data availability. It is expected that each model will perform better under certain conditions or assumptions. As such, modelling during up valley and down valley flow are compared along with stability conditions and binned wind speed.

4.1 Wind Conditions

4.1.1 Data Availability

Given the multiple layers of sensitive filters applied to the data, availability must be considered to provide context for how representative the models are. Availability is calculated after re-sampling to 1 hr period. Over the course of the 7 weeks campaign, 58.9% of the LiDAR RHI scans were suitable to used. Of those suitable data points, 92.3% have a difference in LiDAR and AWS 10 m wind speed measurement less than 3 m/s. 56.0% show wind direction within 30°of the RHI scan heading up or down valley at 10 m and 100 m through 150 m height. 69.4% show wind speeds greater than 2 m/s at 10 m and 100 m through 150 m height. Combining the wind direction and speed filters, leaves 47.6%. 10.9% of the suitable RHI scan points are outside $-0.5 < \mathrm{Ri} < 0.2$ The total availability after quality and usability checks is 26.3% of the data points collected over the summer campaign and re-sampled to 1 hr.

4.1.2 Direction

The wind direction sometimes varies with height in Adventdalen. The variation increases with height as shown in figure 7. While wind direction tends to remain near constant with increasing height, there is a minor trend where the direction at 10 m holds a heading of roughly 310° while at 100 m and above the wind direction varies from 100° to 330°. This trend increases with height as the cluster of points at 310°, 10 m height shift downwards from the 1:1 correlation line. At 150 m height, a hotspot develops around 130° heading indicating opposing flow above the valley floor. Along the 1:1 correlation line, three hotspots are seen: at 310 deg heading, 130 deg heading, and at 220 deg which would be a crosswind. The crosswind is seen at all heights.

Figure 8 further shows that the trend of wind direction aligned up or down valley is common. This further supports the trends seen in the correlation plot above. At 10 m height, the wind direction is typically aligned with Adventdalen. At 100 m and 150 m heights, the wind direction shifts slightly on occasion between 110° and 330°. At 10 m height, the wind direction typically does not deviate from aligning with the valley with the clearest exceptions being on July 11, July 27-30, and August 18. Again, this is not common which aligns with the findings from the correlation plots. The cases of crosswind and flow not aligned with Adventdalen are not being evaluated in this project. Rather, this explanation is to provide context for the low suitable data availability.

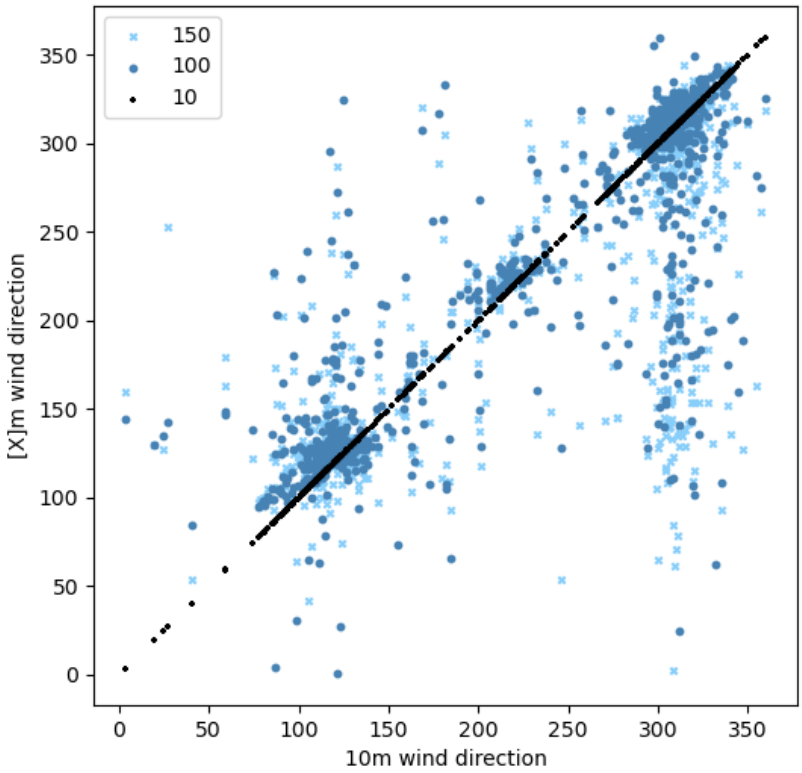

Figure 7: Wind direction correlation at 10 m to 10 m, 100 m, and 150 m heights

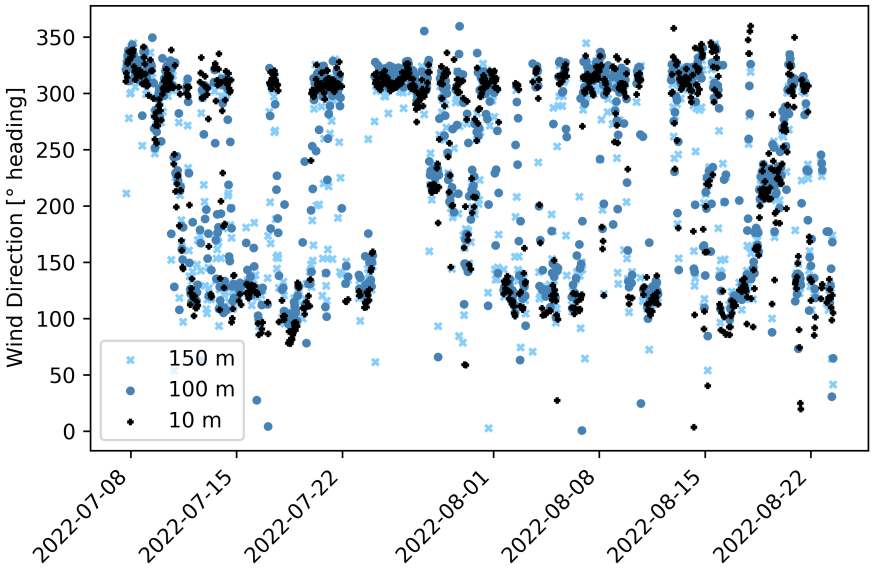

Figure 8: Time series of wind direction at 10 m, 100 m, 150 m heights

4.1.3 Stability Classes

Three stability classes are used for evaluating the models, unstable, neutral, and stable. Figure 9 shows the relation between wind speed and stability class after filtering for low wind speed and wind direction not aligned with the RHI scan direction. The 10 m height wind speed is always greater than the 2 m height wind speed, as expected. Unstable conditions are seen primarily between 3 m/s and 7 m/s wind speed. Neutral conditions are seen throughout all speeds, especially from 4 m/s to 10 m/s. Stable conditions are seen from 1.5 m/s to 5 m/s. 2 m height speeds go below 2 m/s in spite of the filter because the filter is applied at 10 m height. For neutral conditions, the speed increases at a slightly higher rate from 2 m to 10 m height than in the other stability classes (table 6).

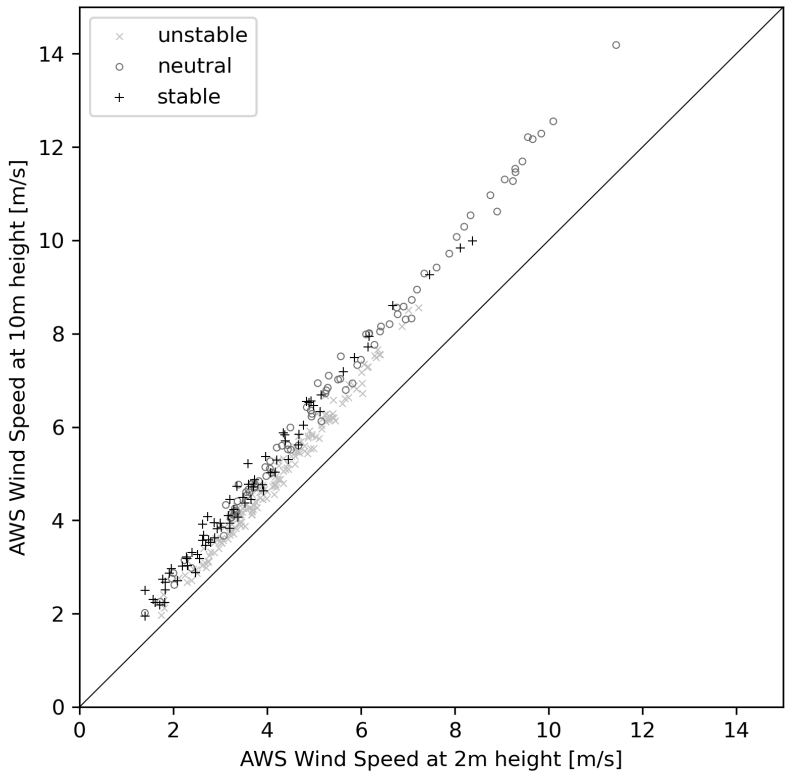

Figure 9: Stability classes based off 2m and 10m heights

Table 6: Slope for 10 m vs 2 m height windspeed in fig. 9

Unstable	Neutral	Stable
1.17	1.21	1.18

4.2 All Wind Profiles

The LiDAR and model profiles are constructed at each point in the timeseries. A correlation plot provides a quick visualization of the performance of each model at 80 m height (fig 10). All models tend to overestimate the wind speed. The IEC model has the highest and most frequent over-estimation. The Sedefian model has the most under-estimation. Both log models show less deviation from the 1:1 correlation line.

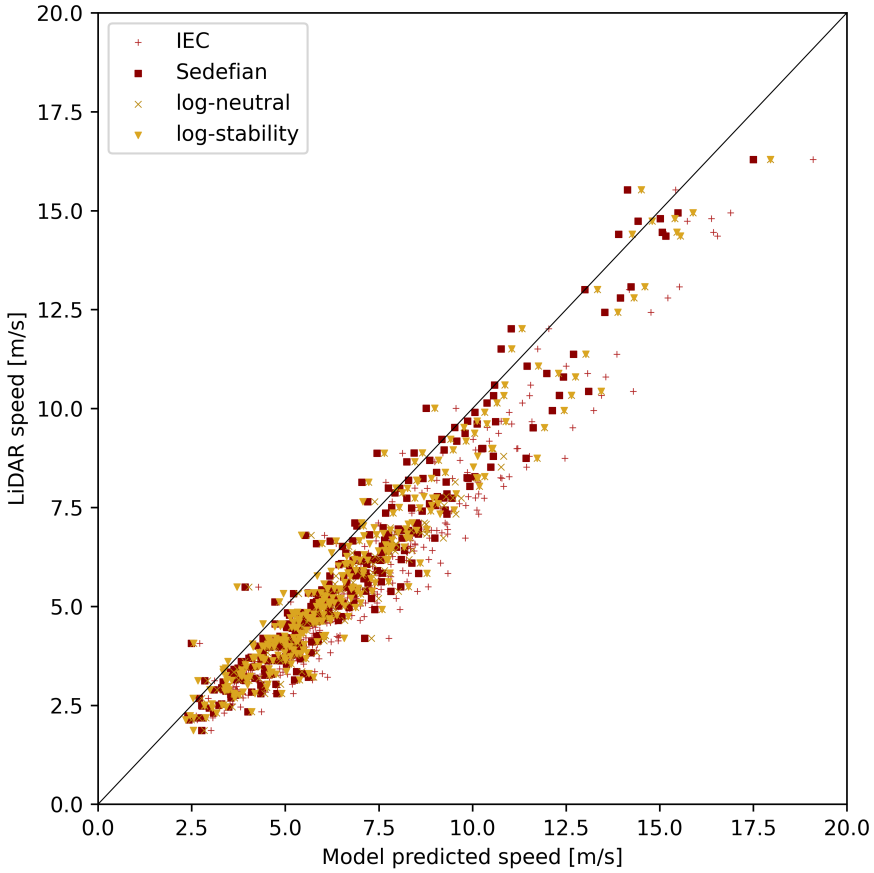

Figure 10: Model to LiDAR profile correlation for all suitable profiles at 80 m height

The profile of medians taken over the data collection period is used for overall comparison (fig 11). The median is chosen over the mean as the median will select the most common values with less influence from extreme cases. Over the duration of the summer LiDAR campaign, the log-stability model most closely matches the measured profile up to 120 m height. The IEC model has the highest median estimated wind speed and as expected, performs the worst. However, the Sedefian model performs similarly to the log-stability model over the entire campaign. Of note, the measured profile from LiDAR shows a general slight decrease in wind speed with height starting at 50 m. As these models all assume an increase in wind speed with height, it is then expected that a good fit is not possible.

The difference in wind speed profiles highlights the significance of over estimation of the wind speed using each method (fig 12). The Sedefian model performs nearly as

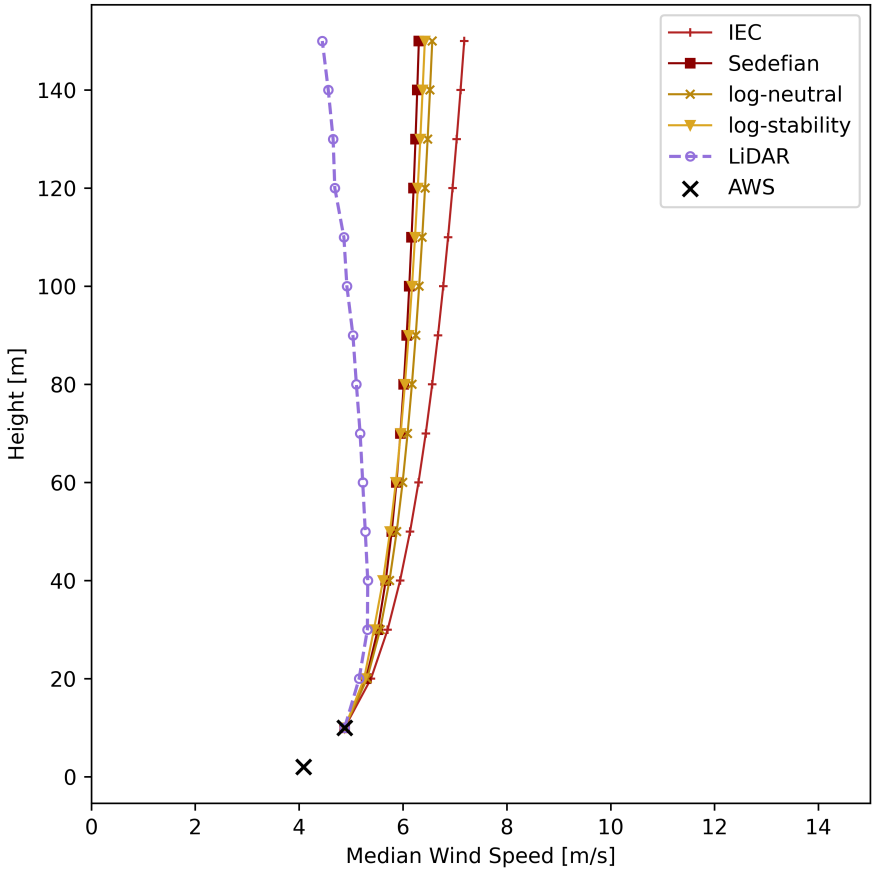

Figure 11: Median wind speed for all suitable profiles

well as the log-stability model, staying under 0.5m/s difference up until just over 50 m. The log models run nearly parallel due to the stability correction present in the log-stability model. This is due to the correction term being added and multiplied by the same scalar u_r (6).

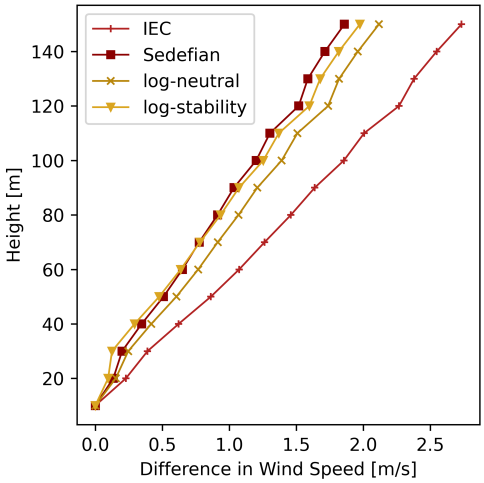

Figure 12: Median difference of models to LiDAR wind speed for all suitable profiles

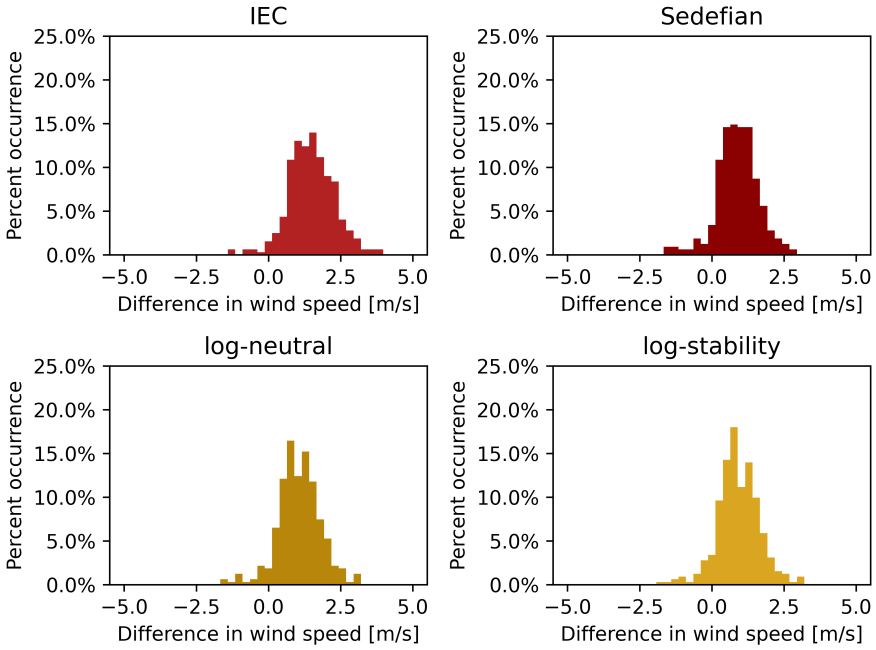

Figure 13: Percent distribution of difference in model vs LiDAR wind speed for all suitable profiles at 80m height

The percent distribution of the difference in model from LiDAR wind speed at 80 m height (fig 13) shows how frequently and by how much each model differs from the LiDAR profile. The percent is taken from the total number of suitable data points used in modeling the all case. All models have a forward-weighted distribution (meaning the model tends to overestimate). The IEC has a flatter profile indicating higher variance in the difference of model wind speed from the LiDAR wind speed. The Sedefian model has a more symmetrical distribution centered around 1.0 m/s. The shape of the distribution is sharper indicating less variance than the IEC model. Both log models have an even sharper distribution and are also centered around 1.0 m/s. The approximately 18% spike around 0.8 m/s for the log-stability model further indicates low variance.

Profiles of wind power density are shown in (fig 14). The wind speed cubed (17) has significant impact on the model predicted wind power density as shown in figure 15. At 80 m height, the median of the difference in model predicted vs LiDAR based wind power density is 50 W/m^2 for the log-stability model while 45 W/m^2 for the Sedefian model (table 7). The standard deviation from the mean shows the breadth of variation in power density over the 7 weeks campaign (fig 15). While the mean difference and standard deviation for the Sedefian and log-stability models are very nearly the same, the median difference in power density is a bit higher with the log-stability model overestimating by 111% more than the Sedefian model. This further shows that power density is a key metric. The Sedefian model has the least standard deviation from the mean while IEC varies most. Both log models have slightly more deviation than the Sedefian model with 0.73 m/s as opposed to 0.72 m/s for the Sedefian model. This corresponds to 116 W/m^2 and 133 W/m^2, respectively.

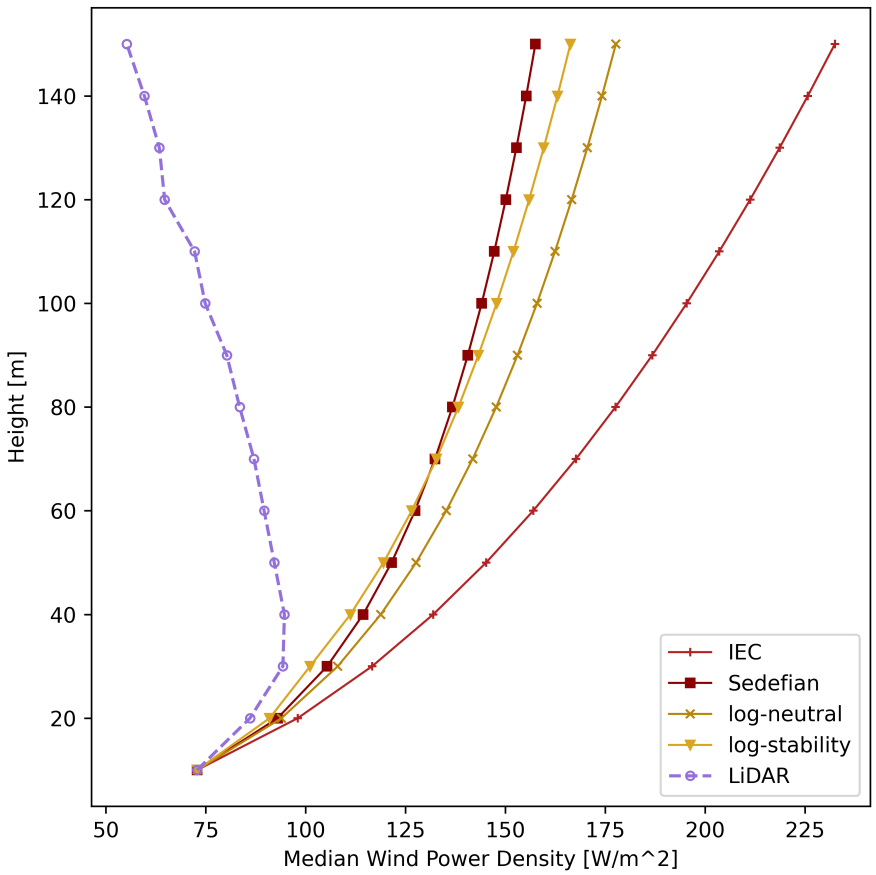

Figure 14: Median wind power density for all case

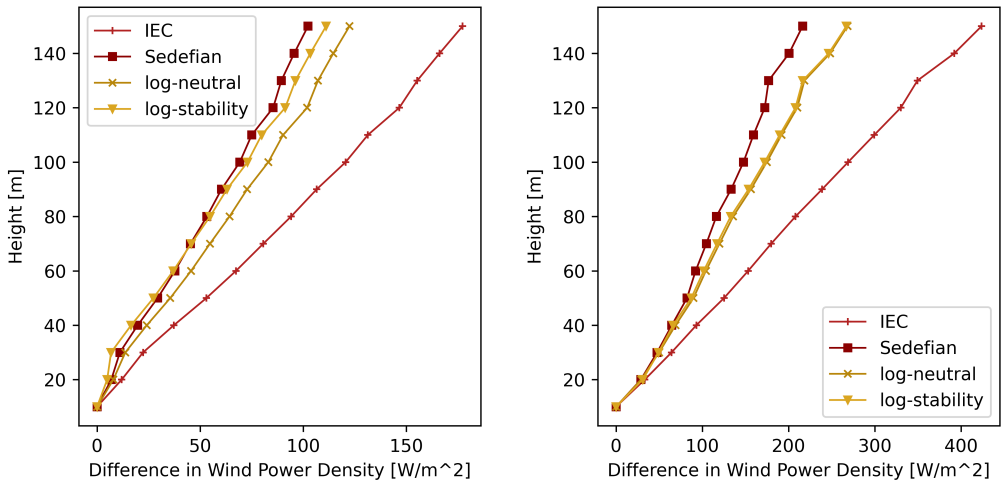

(a) Median of difference in power density of models from LiDAR for all case

(b) Standard deviation of difference in wind power density of models from LiDAR for all case

Figure 15: Comparison of power density profiles using median of difference from LiDAR and standard deviation of that difference

Table 7: Statistical values for all study case when comparing model to LiDAR profiles at 80 m height

Method	IEC	Sedefian	log-neutral	log-stability
Mean Dif. [m/s]	1.5	0.89	1.1	0.91
Std. Dev. [m/s]	0.79	0.72	0.73	0.73
r^2	0.6	0.82	0.77	0.81
Median Dif. Power Density [W/m^2]	87	45	58	50

4.3 Effect of Up Valley vs Down Valley Flow

Up valley flow occurs for 72.7% of the evaluated points and down valley flow for the remaining 27.3%. Figure 16 compares the model to LiDAR correlation for the two scenarios. Up valley shows tighter correlations and generally lower speeds centered around 6 m/s while down valley has a full breadth of wind speeds for the campaign with speeds centered around 10 m/s. Table 8 shows the statistics for the up valley case while table 9 shows the statistics for the down valley case. Up valley flow has very poor correlations for all models. Sedefian and log-stability models have the same mean difference and median difference in power density of 1.0 m/s and 48 W/m^2, respectively. Down valley flow has much better correlations with r^2 slightly higher for Sedefian than the log models. The Sedefian model also has significantly lower mean difference in wind speed and median difference in power density compared to both log models. The up valley case had primarily unstable conditions, 67.5% of the time then 17.1% stable conditions and 15.4% neutral conditions. The down valley case had primarily neutral conditions, 60.2% of the time then 37.5% stable conditions and 2.3% unstable conditions.

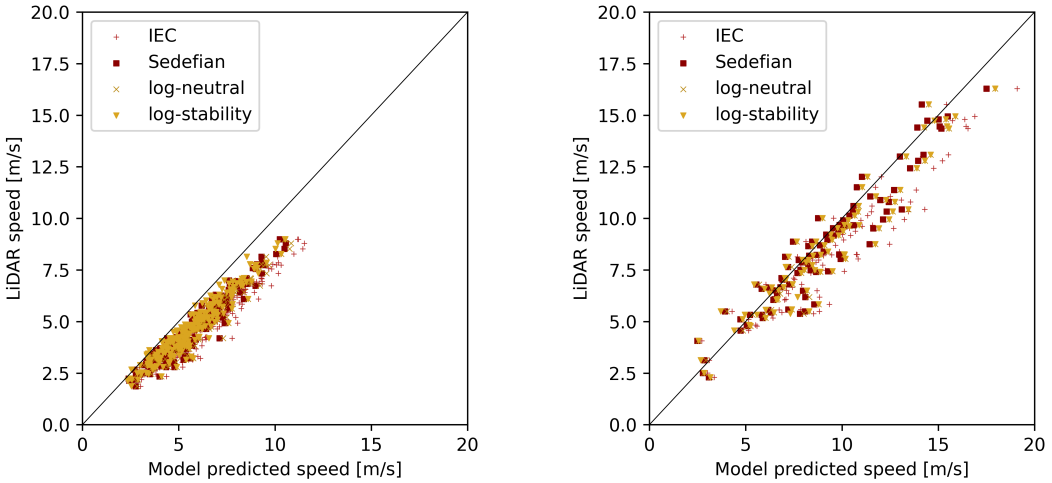

(a) Up valley flow at 80 m

(b) Down valley flow at 80 m

Figure 16: Model to LiDAR correlation for up and down valley cases

The median wind power density is significantly different between up valley and down valley flow due to overall difference wind speed. For up valley flow at 80 m height, the Sedefian model predicts slightly lower energy density than the log-stability model

Table 8: Statistical values for up valley flow when comparing model to LiDAR profiles at 80 m height

Method	IEC	Sedefian	log-neutral	log-stability
Mean Dif. [m/s]	1.6	1.0	1.2	1.0
Std. Dev. [m/s]	0.61	0.5	0.53	0.54
r^2	-0.32	0.37	0.2	0.38
Median Dif. Power Density [W/m^2]	78	48	56	48

Table 9: Statistical values for down valley flow when comparing model to LiDAR profiles at 80 m height

Method	IEC	Sedefian	log-neutral	log-stability
Mean Dif. [m/s]	1.3	0.46	0.7	0.65
Std. Dev. [m/s]	1.1	1.0	1.0	1.0
r^2	0.69	0.87	0.83	0.84
Median Dif. Power Density [W/m^2]	174	36	61	61

with 105 W/m^2 and 108 W/m^2, respectively. However, LiDAR predicts a median energy density of 58 W/m^2, merely slightly over half the model predicted power. For down valley flow, both log models near perfectly overlap suggesting dominant neutral stability. The decrease in wind speed with height for LiDAR starts at 70 m height as opposed to 50 m height for up valley so the difference in predicted energy density is much less. The Sedefian model has a lower estimate than the log models with 401 W/m^2 and 433 W/m^2, respectively. LiDAR predicts 347 W/m^2 which is closer than in the up valley but still significantly less.

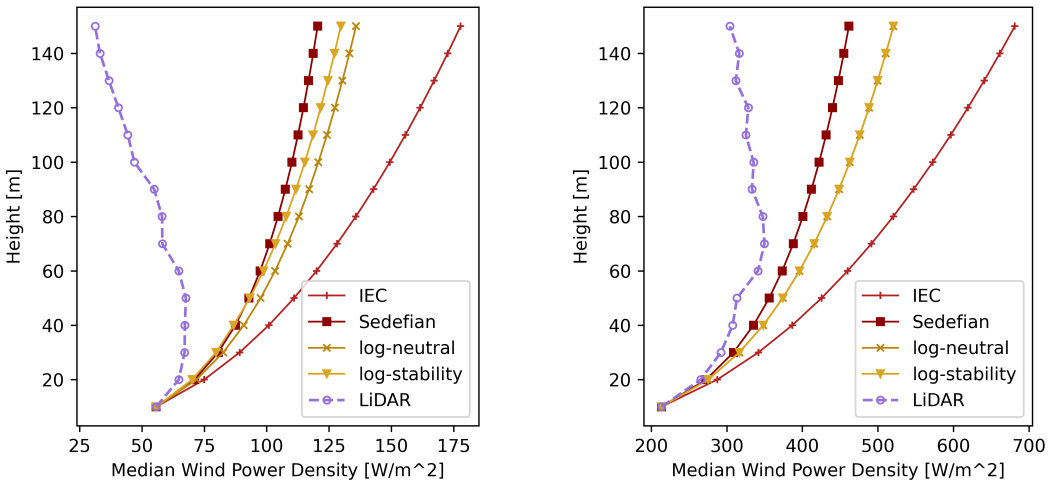

(a) Up valley flow

(b) Down valley flow

Figure 17: Median wind power density for up and down valley cases

4.4 Effect of Stability

Stability is a key consideration for all models. For the basic power and log laws, neutral stratification is assumed. Therefore it is useful to compare the impact of

stability on model predictions. For comparison convenience, neutral condition is defined as $-0.025 < \text{Ri} < 0.025$. Stable conditions are when $0.025 \geq \text{Ri} < 0.2$ and unstable are when $-0.5 < \text{Ri} \leq -0.025$. Unstable conditions occurred 49.7% of the time; neutral occurred 27.6%, and stable occurred 22.7%. The correlation plots for each are shown in figure 18. As seen in the stability correlation plot above, unstable conditions occur at lower speeds, stable conditions at lower through middle speeds, and neutral conditions throughout all speeds.

The coefficient of determination for all models in the unstable case are very poor with the highest being log-stability with $r^2 = 0.39$ (table 10). The correlation is significantly better for the neutral case (table 11) where the best correlation is for Sedefian model with $r^2 = 0.90$. As expected, both log models perform exactly the same as the correction term is 0 per definition. Also, both log models have slightly lower correlation than the Sedefian model. The stable case (table 12) has worse correlation coefficients than the neutral case for all models. In the stable case, the log-stability model has better correlation than the log-neutral model as expected given the correction term. The mean difference in wind speed decreases for all models going from the unstable, to neutral, to stable case. The standard deviation decreases for all models in the same order. However, the lowest mean speed is for stable conditions, then unstable and finally neutral conditions indicating that neutral conditions have the tightest fit. Of note is that the IEC model has the highest standard deviation in all cases with the Sedefian model having the lowest standard deviation, even when out-performed in terms of correlation or mean difference. And while the unstable case has very poor coefficients of determination, it has the lowest standard deviations across all models.

Table 10: Statistical values for unstable conditions when comparing model to LiDAR profiles at 80 m height

Method	IEC	Sedefian	log-neutral	log-stability
Mean Dif. [m/s]	1.7	1.1	1.3	1.1
Std. Dev. [m/s]	0.6	0.51	0.53	0.54
r^2	-0.38	0.34	0.16	0.39
Median Dif. Power Density [W/m^2]	98	58	68	53

Table 11: Statistical values for neutral conditions when comparing model to LiDAR profiles at 80 m height

Method	IEC	Sedefian	log-neutral	log-stability
Mean Dif. [m/s]	1.5	0.71	0.93	0.93
Std. Dev. [m/s]	0.87	0.82	0.83	0.83
r^2	0.76	0.9	0.87	0.87
Median Dif. Power Density [W/m^2]	119	48	65	65

In the unstable and stable cases, the log-stability model has the closest prediction of wind energy density up to 120 m (fig 19). The fit is not significantly different above this height. In the neutral case, the Sedefian model performs noticeably better. The decrease in wind speed with height for LiDAR profiles once again accentuates the

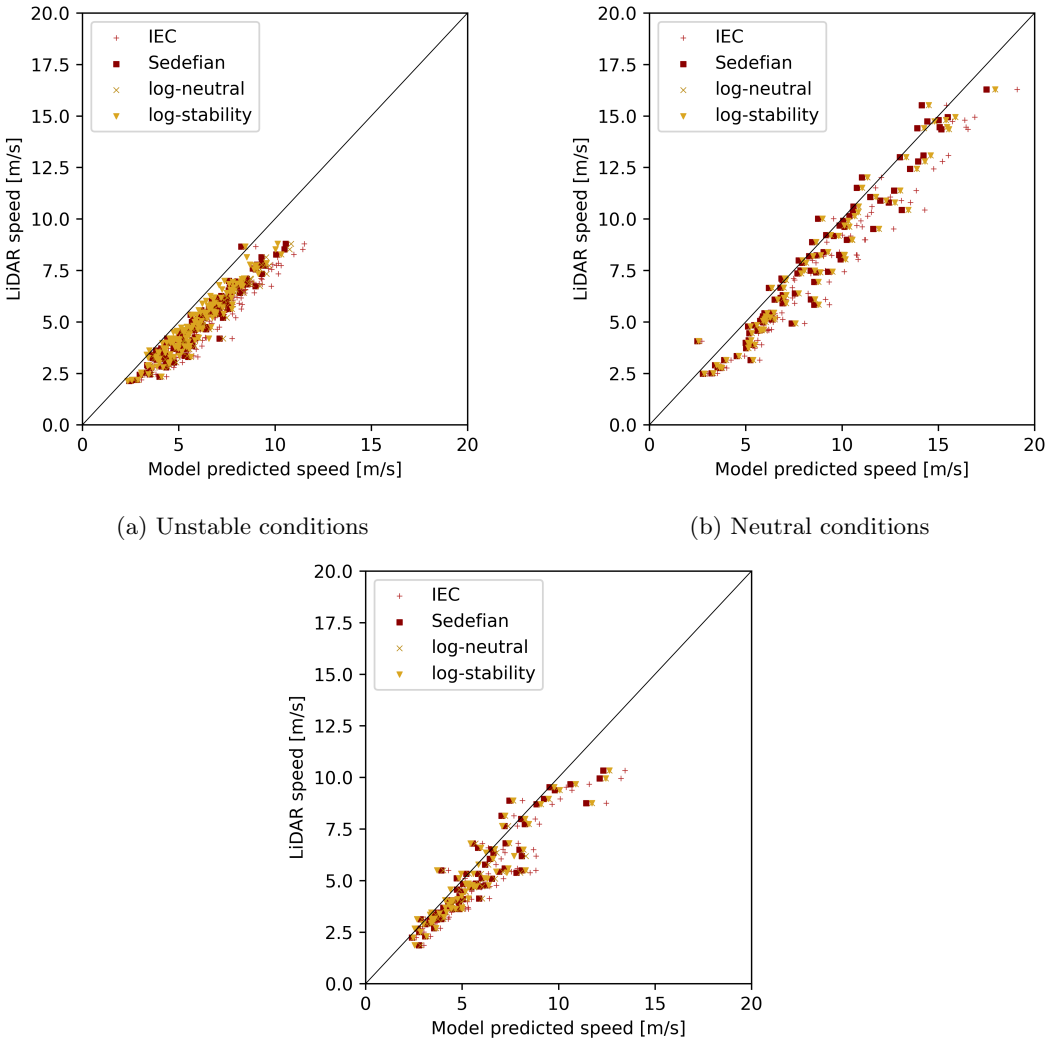

(a) Unstable conditions

(b) Neutral conditions

(c) Stable conditions

Figure 18: Model to LiDAR profile correlation for unstable, neutral, and stable stability conditions at 80 m height

Table 12: Statistical values for stable conditions when comparing model to LiDAR profiles at 80 m height

Method	IEC	Sedefian	log-neutral	log-stability
Mean Dif. [m/s]	1.1	0.59	0.74	0.59
Std. Dev. [m/s]	0.92	0.83	0.85	0.85
r^2	0.53	0.77	0.72	0.76
Median Dif. Power Density [W/m^2]	48	21	31	20

generally poor model fits. For unstable conditions, the decreases starts around 50 m. For stable conditions, the decrease starts around 70 m. For neutral conditions, the decrease appears to also start around 70 m. The jagged shape of the curve is due to high variance as seen in the correlation plot.

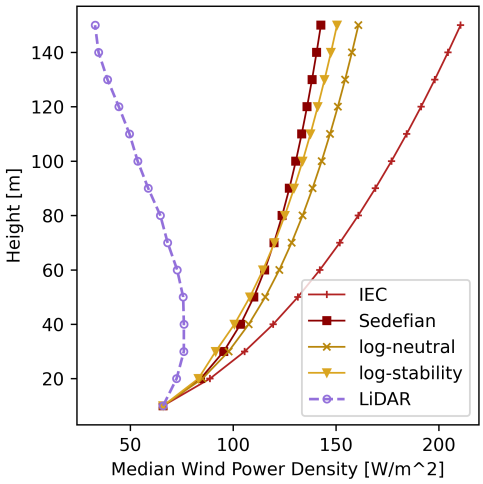

(a) Unstable conditions

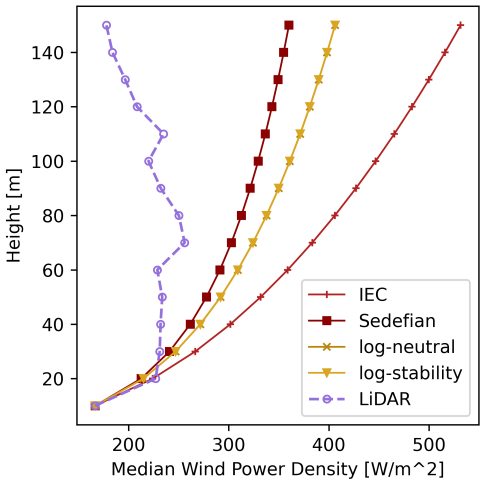

(b) Neutral conditions

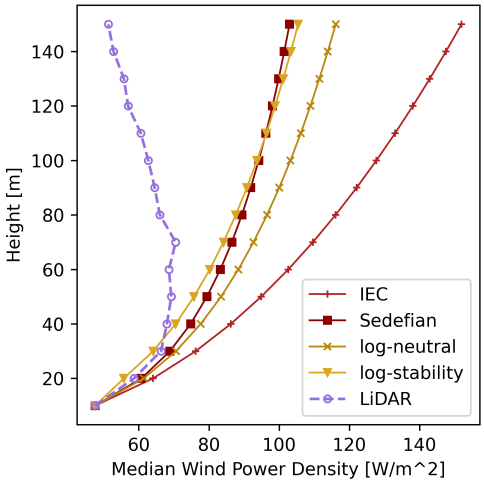

(c) Stable conditions

Figure 19: Median wind power density for unstable, neutral, and stable stability conditions

4.5 Effect of Wind Speed

Of the total suitable data set, 60.6% were in class 0-3, 27.3% were in class 4, 8.7% were in class 5, and 3.4% were in class 6+. The speeds are shown in the plot descriptions. The correlation of model to LiDAR wind speed is shown in figure 20. The variance increases with increase in speed across the models. The IEC model is seen clearly as the worst performing while the Sedefian and both log models require closer investigation.

In each speed class, the correlation is very poor for all models with most values being negative and the highest value being 0.34. Due to the dependence of wind energy density on velocity, not much can be said about the median difference in predicted wind energy density of the models from the LiDAR when comparing speed classes. Nonetheless, the IEC model has a median difference in wind energy density approximately two times the other model's difference in all speed classes.

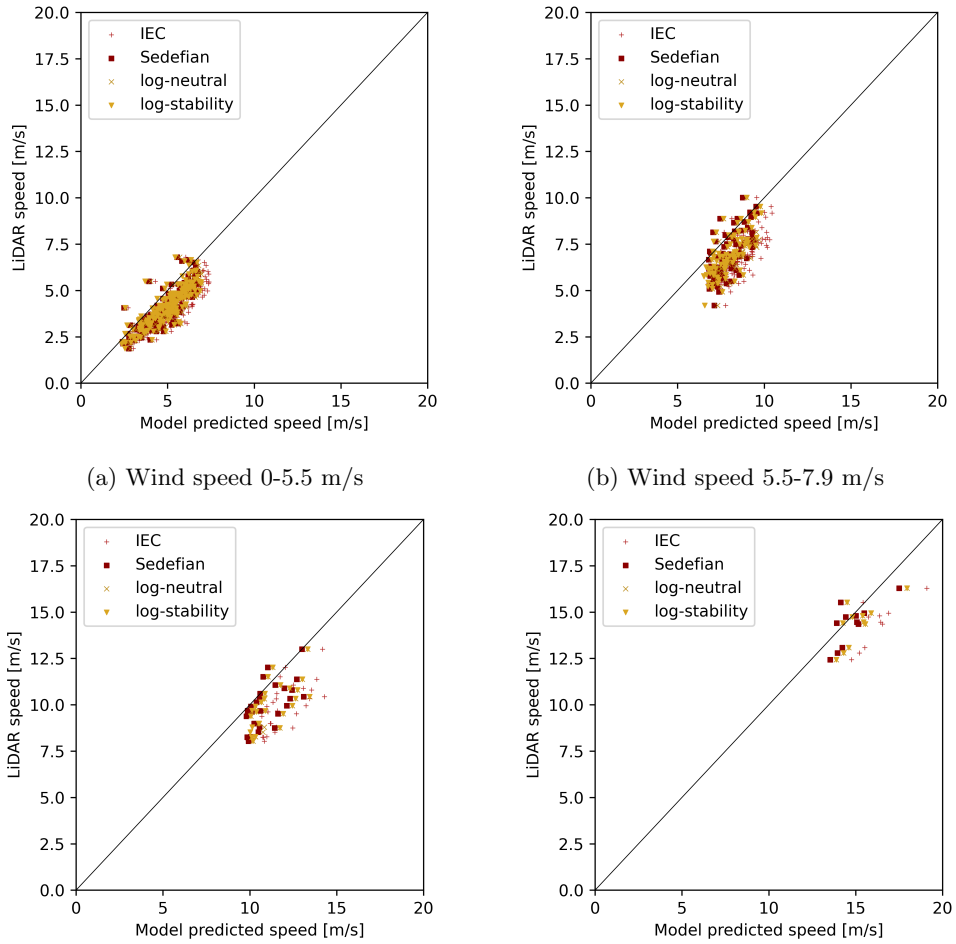

(a) Wind speed 0-5.5 m/s

(b) Wind speed 5.5-7.9 m/s

(c) Wind speed 7.9-10.7 m/s

(d) Wind speed 10.7+ m/s

Figure 20: Model to LiDAR profile correlation at 80 m height for four different speed classes based off 10 m height AWS wind speed: a) 0-5.5 m/s, b) 5.5-7.9 m/s, c) 7.9-10.7 m/s, d) 10.7+ m/s

Table 13: Statistical values for 0-5.5 m/s wind speed when comparing model to LiDAR profiles at 80 m height

Method	IEC	Sedefian	log-neutral	log-stability
Mean Dif. [m/s]	1.3	0.82	0.95	0.81
Std. Dev. [m/s]	0.62	0.57	0.59	0.62
r^2	-0.94	0.03	-0.21	-0.0091
Median Dif. Power Density [W/m^2]	60	34	41	32

Table 14: Statistical values for 5.5-7.9 m/s wind speed when comparing model to LiDAR profiles at 80 m height

Method	IEC	Sedefian	log-neutral	log-stability
Mean Dif. [m/s]	1.8	1.0	1.3	1.0
Std. Dev. [m/s]	0.86	0.86	0.86	0.8
r^2	-2.0	-0.41	-0.78	-0.32
Median Dif. Power Density [W/m^2]	192	108	131	109

Wind speed was also evaluated using overlapping divisions of 0-7 m/s, 5-11 m/s, 7-13 m/s, and 9+ m/s. Wind speed was also evaluated using quartiles. In both of

Table 15: Statistical values for 7.9-10.7 m/s wind speed when comparing model to LiDAR profiles at 80 m height

Method	IEC	Sedefian	log-neutral	log-stability
Mean Dif. [m/s]	2.1	1.1	1.4	1.3
Std. Dev. [m/s]	1.0	0.98	0.99	0.96
r^2	-2.6	-0.41	-0.89	-0.76
Median Dif. Power Density [W/m^2]	427	236	287	259

Table 16: Statistical values for 10.7+ m/s wind speeds when comparing model to LiDAR profiles at 80 m height

Method	IEC	Sedefian	log-neutral	log-stability
Mean Dif. [m/s]	1.8	0.42	0.8	0.8
Std. Dev. [m/s]	0.87	0.84	0.85	0.85
r^2	-2.1	0.34	-0.048	-0.048
Median Dif. Power Density [W/m^2]	892	251	423	423

these cases, the trends between increasing wind speed and model fit were less clear than in the case shown using the Beaufort classes. An increase in r^2 values was seen using the overlapping divisions indicating that at this limited quantity of data, the r^2 is driven more by the number of data points than by the case parameters.

The shape of the LiDAR profile shows an increasingly strong low level jet with increasing speed. The height of decreasing wind speed increases with increasing wind speed, going from 40 m to 50 m to 60 m to 90 m. As the speed class increases, the LiDAR profile approaches the log laws. The log-neutral and log-stability models approach closer to each other with increasing speed until they overlap at 7.9+ m/s. The overlap indicates primarily neutral conditions at higher speeds as shown in the stability correlation plot shown in (fig 18). The shape of the median LiDAR profile also gets increasingly jagged as the variance increases with increasing speed. In the highest speed class, the profiles suggest the log models have the best fit.

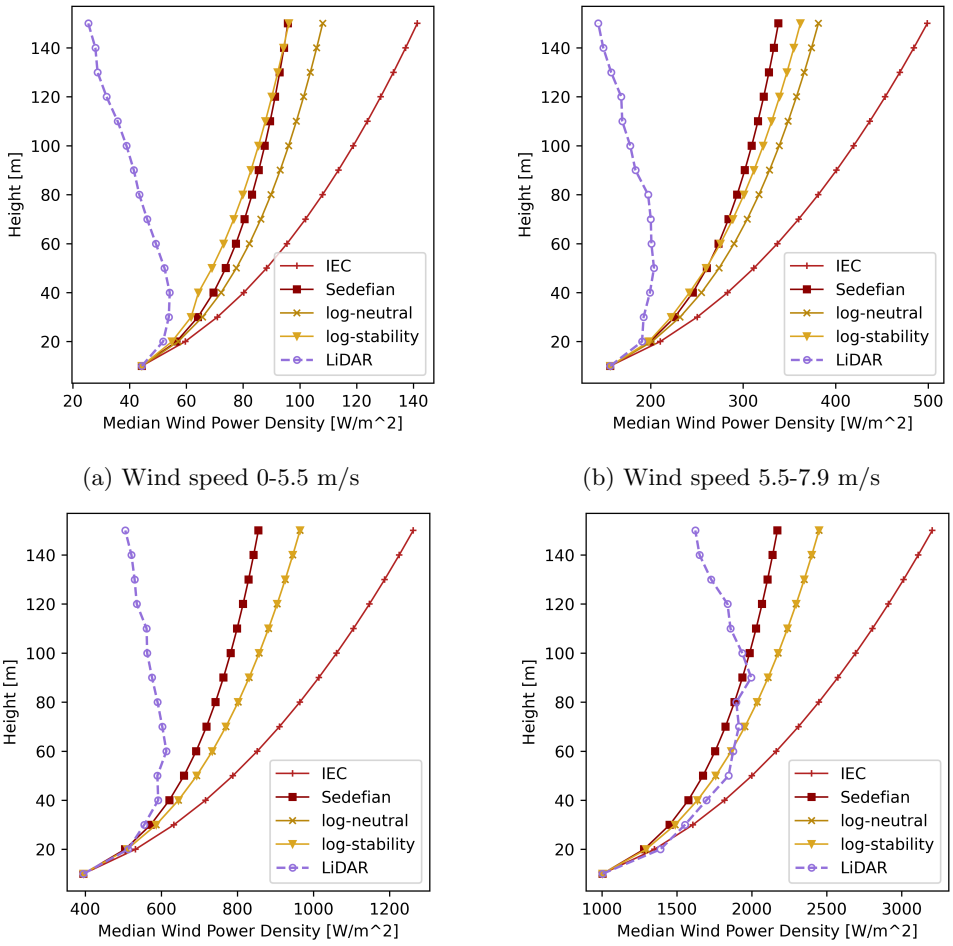

(a) Wind speed 0-5.5 m/s

(b) Wind speed 5.5-7.9 m/s

(c) Wind speed 7.9-10.7 m/s

(d) Wind speed 10.7+ m/s

Figure 21: Median wind power density for four different speed classes based off 10 m height AWS wind speed: a) 0-5.5 m/s, b) 5.5-7.9 m/s, c) 7.9-10.7 m/s, d) 10.7+ m/s

5 Discussion

The Sedefian and log-stability models have the best performance as seen throughout the results. As such, they are the focus of discussing the impacts of each case. Nonetheless, each model's performance is summarized. The baseline LiDAR is first discussed noting a median decrease in wind speed with increasing height. While this presents challenges in evaluating model performance, the models are compared noting their sensitivity to error, impact of the explored cases across models, and general estimation at 80 m height across models. Sensitivity referring to how the estimated wind speed varies with difference in wind measurement. Error referring to the difference in wind for any reason including instrument error and large variance in measurements which could affect roughness length calculation.

5.0.1 Baseline LiDAR Profiles

The median decrease in wind speed with increasing height defies the basic assumption of all models investigated as part of this project, that wind speed increases with increasing height (fig 11). While some cases, such as neutral stability, have strong correlations, the quality of model fit for unstable vs stable conditions is inverse from those typically found in literature. The median decrease in wind speed with height is likely caused by a frequent low-level jet. Note that the cause and modelling of low-level jets are not explored in this project. Simply, it is an observed phenomena which much be acknowledged as it is outside the basic assumption of all models tested: increasing wind speed with height.

Kilpeläinen et al. (2012) investigated the occurrence and core height of LLJs in Kongsfjord on Spitsbergen. The geography there is similar to that found in Adventfjord and Adventdalen. The core height is the point of local maxima where the wind speed starts to decrease with increasing height. It was found that 53% of the observations contained an LLJ with the core height often being ≤ 100 m. This validates the median LiDAR profile showing decreasing wind speed with increasing height. As such, direct comparisons from the LiDAR to model profile shape are limited. While the profile shape and percent difference are not directly evaluated for the reasons above, the baseline LiDAR provides a reference point to base model sensitivity off of. This reference point is used to show error as defined above.

5.1 Study Case Findings

5.1.1 Up vs Down Valley Flow

Up and down valley flow are driven by different features. Up valley flow is influenced by Adventfjord and Isfjord beyond, two large bodies of water. Down valley flow is influenced by the broad valley Advendalen and its' surrounding mountain features such as plateaus, valleys, and gullies. While the models themselves are not tuned to surrounding terrain features lying several hundred meters and beyond the AWS, investigating up and down valley flow provide insight to the specific context

of LiDAR profiles. And, more relevant to this project, they can provide insight to model performance.

The down valley profiles (fig 17) are similar to the neutral condition profiles (fig 19). Higher wind speeds tend to correlate with neutral stability within this dataset (fig 18) so this is expected. The up valley profiles appear to match a mix of stable and unstable conditions. The median LiDAR profile better matches the unstable condition profile while the median model profiles, when compared to each other, more closely match the stable condition profiles.

5.1.2 Stability

As expected, model performance varies through the stability classes. Best performance for all is under neutral conditions and worst is for unstable conditions in terms of correlation (table 11). However, the unstable case has the lowest standard deviations indicating low sensitivity to error and good fit to a model, albeit a different one (table 10). The stable condition case lies in the middle for correlation values and has the highest scatter indicating low reliability for all models (table 12). It also has mixed mean difference for the different models indicating higher model sensitivity to stable conditions.

The results for the unstable condition case match the findings of Newman and Klein (2014). The power law, while assuming neutral stratification, tends to have a less scattered fit than in neutral conditions and especially more than stable conditions. They also found that unstable conditions tended to underestimate while stable conditions tended to overestimate. This is not seen in the results discussed here due to the wind speed tending to decrease with height. All of the explored models assume an increase in wind speed with height.

The standard deviation is a key indicator for this analysis since it shows how consistent the model is in it's prediction. This is necessary as the LiDAR cannot fully be relied on for evaluation. High standard deviation means the model does not closely follow a trend related to the LiDAR while low standard deviation means the model closely follows a trend. High standard deviation indicates high sensitivity of the model to error. This metric works regardless of how good the model fit is. In the stability cases, the standard deviation is lowest for unstable conditions (table 10). This indicates the models are well-suited to unstable conditions as found by Newman and Klein (2014) with regard to log law models. While the correlation is low, the models can be tweaked or a new model developed since some correlation is shown to exist.

The standard deviation increases with stability indicating increased sensitivity to error (tables 11, 12). The poorer fit in stable conditions for log law models also matches the findings of Newman and Klein (2014). There is a net increase in wind speed going from unstable to neutral conditions. However, this trend does not continue into stable conditions where the wind speeds are similar to the unstable case. This indicates that model reliability decreases with increased stability. The models are best tuned to neutral conditions but the Sedefian and log-stability model can

produce good results in unstable conditions. The Sedefian model is better suited for the neutral case than log-stability model.

5.1.3 Wind Speed

Wind speed classes do not reveal a direct trend in model performance for any of the models explored here. All have poor correlation values (tables 13, 14, 15, 16). The mean difference and standard deviation appear to increase with increase in wind speed, as would be expected, but then decrease significantly for the highest speed class. Both are likely caused by too few points, albeit in different ways.

Poor correlation could be due to too small a range of wind speeds. In the case here, the scatter of model vs LiDAR wind speeds is rather like a blob than a long, thin cluster for all speed classes. Visually, one would expect poor correlation values for each category then. Attempts were made to improve the range of values by using overlapping categories (e.g. 0-5 m/s, 3-7 m/s, 5-9 m/s, and 7+ m/s) or quartile divisions of wind speed. Using both methods, the affect of wind speed was less clear with no improvement to correlation coefficients. Likely, the cause was that the highest speed class of both approaches were dominated by lower wind speeds than those in Beaufort 6+ division. As such, the lower limit of their highest speed class was not sufficiently high enough to capture the relationship between higher wind speeds and neutral stability. Based on the stability correlation plot (fig 18), neutral stability dominates at 8+ m/s. Using quartiles, the 0.75 quartile is at 6.3 m/s which is significantly less than the point of dominate neutral stability. And with overlapping divisions, an upper speed class starting at 7 m/s, for example still has a low percentage of points leading to poor correlation values and unclear trends again.

One correlation can be drawn from using the Beaufort speed classes, however. With increase in wind speed, an increase in the occurrence of neutral stability is seen. This was earlier shown in figure 18 where primarily neutral stability was seen at higher wind speeds. In the wind power energy density profiles (fig 21), the log-neutral and log-stability models grow closer to overlapping with increasing wind speed until they overlap from 10.7+ m/s. At the highest speed class, the median of log models overlap with the median of LiDAR near perfectly. The Sedefian model under-performs in the highest speed class as the increasing wind speed portion of the profile extends up high enough that the decreasing portion no longer dominates the comparison.

Emeis (2005) notes that with higher wind speeds stability conditions tend to become neutral. This matches the conditions described prior where the highest wind speeds all occurred under neutral conditions. This also explains the trend seen here where model performance decreases with speed until relatively high (10.7+ m/s) wind speeds are reached at which point the performance is significantly improved. Wind speed still should not be used as a filter for selecting models, but does provide insight to their performance. Stability conditions appear to be dependent on wind speed and therefore should be used for selecting models.

5.2 Models

5.2.1 IEC Power Law

The IEC model has very poor performance when compared to both the LiDAR baseline and the other tried models. Not only is the difference from baseline poor, 1.50 m/s, the standard deviation is the highest in all cases. There is an overestimation of 82.4 W/m^2 on average or 123% (61.0 W/m^2 and 133% for median) at 80 m height when compared to the best fitting model. Compared to the LiDAR, the IEC model is 135 W/m^2 or 219% greater on average. Then, the high standard of deviation means a simple scalar cannot be used to correct the model as the model fit varies too much. This contrasts with the findings of Sedefian (1980) where this model is described as "conservative but reasonable". The results here show a model far from conservative as it strongly tends to highly overestimate the wind speed and there for power density.

There are several key contributors to the IEC model results. The model assumes neutral stratification and has no correction for other conditions. While neutral stability occurred roughly 1/4th of the time, the IEC model still overestimated the wind speed and with the highest mean difference (table 11). However, the neutral case did have the best fit for the IEC model compared to all other cases. The high mean difference coupled with high standard deviation indicates that in spite of the fitness, the model was sensitive to error. In the neutral case, the IEC model was significantly outperformed by all other models as also shown by Newman and Klein (2014).

The high overestimation of the IEC model found here contrasts with the findings of Sisterson et al. (1983) where they found the IEC model to underestimate the wind speed by 15% and therefore wind power density by 40%. The underestimation was attributed to stable conditions. However, their study site contained high vegetation and therefore a much larger roughness length than in Adventdalen. It is then notable that in Adventdalen the median IEC profile overestimates wind speed even at heights where the wind speed still increases with height. This is attributed to the very smooth terrain.

The shear exponent, $\alpha = 1/7$, is empirically derived for neutral conditions over smooth terrain (Peterson & Hennessey, 1978). This is another large contributor to the model's performance. The value determined for the roughness length in Adventdalen is approximate to the smooth class given by Wieringa (1986). Given the high overestimation of the IEC model even under the assumed neutral conditions over smooth terrain, it is inferred that there are other factors to consider. The shear exponent has been shown to depend on a variety of factors including terrain features, roughness, and stability (Sedefian, 1980). In the case of Sedefian, the shear exponent is also a function of height. As such, the shear exponent is not constant but rather continuously decreasing with height. This function is factored into the here-named Sedefian model, also explored in this project.

5.2.2 Sedefian Model

The Sedefian model tends to have lower standard deviation values (tables 7-16). This makes it well suited to use when errors can be large. Using 10 m data can have a significant impact on estimates at greater heights as found by Motta et al. (2005). They saw non-correlated variation in difference between the model and observed wind speed at 70 m across different sites.

In stable conditions the Sedefian model performs well and even identically to the log-stability model at 80 m height (table 12). At 20 m and 30 m height the Sedefian model more closely matches the LiDAR profile (fig 19). This contrasts with other findings mentioned earlier which state these models perform worst under stable conditions. The flip in performance hierarchy is attributed to the decrease in wind speed with increasing height.

The Sedefian model also tends to have lower wind speed estimates. Under neutral conditions they are close to the log-stability model (fig 19). This matches the derivation proposed by Sedefian (1980) and used here. Emeis (2005) further explores this method. He finds that under neutral conditions the fit between power and log laws become closer with decrease in roughness length. As a low roughness length fitting a very smooth surface is used in this project, the findings here match. Given that, and the lower sensitivity to error, the Sedefian model is preferred under neutral conditions. Lopez-Villalobos et al. (2022) also found that the Sedefian method was preferred if wind measurements were available at two heights. However, they also suggested using the log law if temperature was also available.

5.2.3 Log Law

While two variations of the log law are investigated, they can be treated as nearly the same given that the stability correction term is additive. The log-stability model performs best under neutral conditions, followed by stable conditions (tables 11, 12). Performance is worst for unstable conditions (table 10) contrasting with Newman and Klein (2014) and Van Wijk et al. (1990).

Stable conditions are challenging to model as demonstrated by Optis et al. (2015) as they are highly sensitive to the correction term derived from the wind speed shear. There is debate on which coefficients best suit this term. As such, the Sedefian model is preferred for its' robustness shown with lower standard deviations. However, with future improvements to the correction term, the log law could be the preferred model in all conditions. Optis et al. (2015) found that a simple calculation of the roughness length, the same used in this project, provided the best fit of the correction term.

6 Conclusion

Four methods of extrapolating vertical profiles of horizontal wind speed within the boundary layer using AWS measurements were investigated. A LiDAR campaign was conducted in Adventdalen on Spitsbergen to provide baseline profiles for evaluating the models. A series of quality checks and filters limit profiles to the most direct comparisons between LiDAR scans and AWS data. The median profile constructed from LiDAR scans showed a decrease in wind speed with height. While physical and previously shown to occur in comparable regions, this breaks the foundational assumption of all models tested; that wind speed increases with increasing height.

All methods perform less than satisfactory given decrease in wind speed with height. However, there are clear differences in performance which are summarized in the list below. The IEC model severely overestimates the wind power density with high sensitivity to wind speed error (sensitivity referring to how much the estimation varies for a given measurement difference). The Sedefian model is the least sensitive to wind speed measurement differences. The log-neutral model produces profiles parallel to the log-stability model, as expected. Using a simple factor of safety multiplier may be possible however, the log-neutral model is sensitive also to roughness length. When coupling a best guessed factor of safety with the log-neutral model's sensitivity to roughness length a severe under or over-estimation of the wind power density is likely. However, with the correction term added and further understanding of stable conditions, the log-stability model has the potential to perform better than the Sedefian model. Given the level of uncertainty and unknowns, the Sedefian model is best suited to use in all conditions.

Summary

- The IEC power law model severely overestimates the wind speed in all cases.
- The log-stability model has lowest median wind speed estimation making it the best fit for the LiDAR baseline.
- The log-neutral model estimates in parallel to the log-stability model but is too sensitive to coefficient estimations to leave off the correction term.
- The Sedefian model has the least sensitivity to wind speed error and bias making it ideal for potentially unreliable measurements.

Bibliography

Abolude, A., & Zhou, W. (2017). A preliminary analysis of wind turbine energy yield. *Energy Procedia*, *138*, 423–428. https://doi.org/10.1016/j.egypro.2017.10.189

Arya, S. P. (2001). *Introduction to micrometeorology* (2nd ed). Academic Press.

Beck, H., & Kühn, M. (2017). Dynamic data filtering of long-range doppler lidar wind speed measurements. *Remote Sensing*, *9*(6), 561. https://doi.org/10.3390/rs9060561

de Witt, M., Stefánsson, H., Valfells, Á., & Larsen, J. N. (2021). Energy resources and electricity generation in arctic areas. *Renewable Energy*, *169*, 144–156. https://doi.org/10.1016/j.renene.2021.01.025

Dimitrov, N., Natarajan, A., & Mann, J. (2017). Effects of normal and extreme turbulence spectral parameters on wind turbine loads. *Renewable Energy*, *101*, 1180–1193. https://doi.org/https://doi.org/10.1016/j.renene.2016.10.001

Emeis, S. (2005). How well does a power law fit to a diabatic wind profile. *DEWI Magazine*, *26*, 59–62.

Gualtieri, G., & Secci, S. (2014). Extrapolating wind speed time series vs. weibull distribution to assess wind resource to the turbine hub height: A case study on coastal location in southern italy. *Renewable Energy*, *62*, 164–176. https://doi.org/10.1016/j.renene.2013.07.003

Högström, U. (1996). Review of some basic characteristics of the atmospheric surface layer. *Boundary-Layer Meteorology*, *78*(3-4), 215–246. https://doi.org/10.1007/bf00120937

Design requirements for offshore wind turbines (Standard). (2019). International Electrotechnical Organization. Geneva, CH.

Kalvig, S., Gudmestad, O. T., & Winther, N. (2014). Exploring the gap between 'best knowledge' and 'best practice' in boundary layer meteorology for offshore wind energy: Wave-influenced wind and stability. *Wind Energy*, *17*(1), 161–171. https://doi.org/10.1002/we.1572

Kilpeläinen, T., Vihma, T., Manninen, M., Sjöblom, A., Jakobson, E., Palo, T., & Maturilli, M. (2012). Modelling the vertical structure of the atmospheric boundary layer over arctic fjords in svalbard. *Quarterly Journal of the Royal Meteorological Society*, *138*(668), 1867–1883. https://doi.org/10.1002/qj.1914

Lokalsamfunnsplan. (2023). https://www.lokalstyre.no/energiplan.581707.no.html

Lopez-Villalobos, C., Martınez-Alvarado, O., Rodriguez-Hernandez, O., & Romero-Centeno, R. (2022). Analysis of the influence of the wind speed profile on wind power production. *Energy Reports*, *8*, 8079–8092. https://doi.org/10.1016/j.egyr.2022.06.046

Motta, M., Barthelmie, R. J., & Vølund, P. (2005). The influence of non-logarithmic wind speed profiles on potential power output at danish offshore sites. *Wind Energy*, *8*(2), 219–236. https://doi.org/10.1002/we.146

Murthy, K., & Rahi, O. (2017). A comprehensive review of wind resource assessment. *Renewable and Sustainable Energy Reviews*, *72*, 1320–1342. https://doi.org/10.1016/j.rser.2016.10.038

Newman, J., & Klein, P. (2014). The impacts of atmospheric stability on the accuracy of wind speed extrapolation methods. *Resources*, *3*(1), 81–105. https://doi.org/10.3390/resources3010081

Norwegian Polar Institute. (n.d.). Adventdalen region. Retrieved 30th September 2010, from https://toposvalbard.npolar.no

Optis, M., Monahan, A., & Bosveld, F. C. (2015). Limitations and breakdown of monin-obukhov similarity theory for wind profile extrapolation under stable stratification. *Wind Energy*, *19*(6), 1053–1072. https://doi.org/10.1002/we.1883

Peterson, E. W., & Hennessey, J. P. (1978). On the use of power laws for estimates of wind power potential. *Journal of Applied Meteorology*, *17*(3), 390–394. https://doi.org/10.1175/1520-0450(1978)017⟨0390:otuopl⟩2.0.co;2

Piironen, A. K., & Eloranta, E. W. (1995). Accuracy analysis of wind profiles calculated from volume imaging lidar data. *Journal of Geophysical Research*, *100*(D12), 25559. https://doi.org/10.1029/94jd02605

Platt, S. M., Hov, Ø., Berg, T., Breivik, K., Eckhardt, S., Eleftheriadis, K., Evangeliou, N., Fiebig, M., Fisher, R., Hansen, G., Hansson, H.-C., Heintzenberg, J., Hermansen, O., Heslin-Rees, D., Holmén, K., Hudson, S., Kallenborn, R., Krejci, R., Krognes, T., ... Tørseth, K. (2022). Atmospheric composition in the european arctic and 30 years of the zeppelin

observatory, ny-Ålesund. *Atmospheric Chemistry and Physics*, *22*(5), 3321–3369. https://doi.org/10.5194/acp-22-3321-2022

Rantanen, M., Karpechko, A. Y., Lipponen, A., Nordling, K., Hyvärinen, O., Ruosteenoja, K., Vihma, T., & Laaksonen, A. (2022). The arctic has warmed nearly four times faster than the globe since 1979. *Communications Earth and Environment*, *3*(1), 168. https://doi.org/10.1038/s43247-022-00498-3

Sedefian, L. (1980). On the vertical extrapolation of mean wind power density. *Journal of Applied Meteorology*, *19*(4), 488–493. https://doi.org/10.1175/1520-0450(1980)019⟨0488:otveom⟩2.0.co;2

Sisterson, D., Hicks, B., Coulter, R., & Wesely, M. (1983). Difficulties in using power laws for wind energy assessment. *Solar Energy*, *31*(2), 201–204. https://doi.org/10.1016/0038-092x(83)90082-8

Sjöblom, A. (2014). Turbulent fluxes of momentum and heat over land in the high-arctic summer: The influence of observation techniques. *Polar Research*, *33*(1), 21567. https://doi.org/10.3402/polar.v33.21567

Stull, R. B. (2009). *An introduction to boundary layer meteorology*. Springer.

Van Wijk, A., Beljaars, A., Holtslag, A., & Turkenburg, W. (1990). Evaluation of stability corrections in wind speed profiles over the north sea. *Journal of Wind Engineering and Industrial Aerodynamics*, *33*(3), 551–566. https://doi.org/10.1016/0167-6105(90)90007-Y

Wallenius, T., & Lehtomäki, V. (2015). Overview of cold climate wind energy: Challenges, solutions, and future needs. *Wiley Interdisciplinary Reviews: Energy and Environment*, *5*(2), 128–135. https://doi.org/10.1002/wene.170

Wieringa, J. (1986). Roughness-dependent geographical interpolation of surface wind speed averages. *Quarterly Journal of the Royal Meteorological Society*, *112*(473), 867–889. https://doi.org/10.1002/qj.49711247316

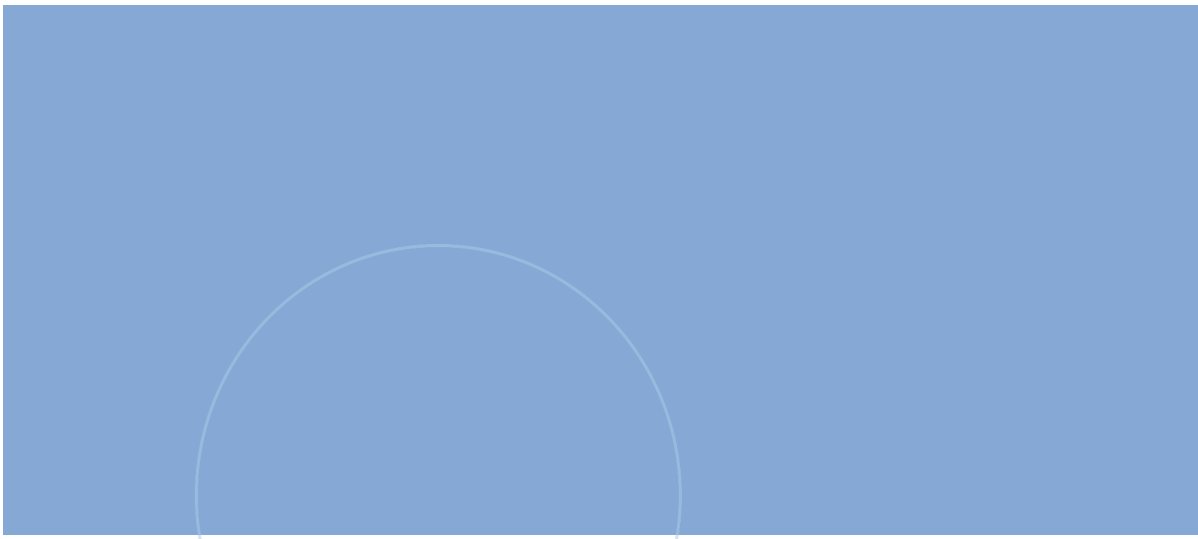

NTNU
Norwegian University of
Science and Technology

UNIS
The University Centre in Svalbard